American Genetic Association

Journal of Heredity, 2020, 147–168
doi:10.1093/jhered/esz076
Original Article
Advance Access publication December 14, 2019

OXFORD

Original Article

ILS-Aware Analysis of Low-Homoplasy Retroelement Insertions: Inference of Species Trees and Introgression Using Quartets

Mark S. Springer, Erin K. Molloy, Daniel B. Sloan, Mark P. Simmons, and John Gatesy

From the Department of Evolution, Ecology, and Organismal Biology, University of California, Riverside, CA 92521 (Springer); the Department of Computer Science, University of Illinois at Urbana-Champaign, Urbana, IL 61801 (Molloy); the Department of Biology, Colorado State University, Fort Collins, CO 80523 (Sloan and Simmons); and the Division of Vertebrate Zoology and Sackler Institute for Comparative Genomics, American Museum of Natural History, New York, NY 10024 (Gatesy).

Address correspondence to M. S. Springer at the address above, or e-mail: springer@ucr.edu.

Address also correspondence to J. Gatesy at the address above, or e-mail: jgatesy@amnh.org.

Received July 13, 2019; First decision 25 August 2019; Accepted December 12, 2019.

Corresponding Editor: William Murphy

Abstract

DNA sequence alignments have provided the majority of data for inferring phylogenetic relationships with both concatenation and coalescent methods. However, DNA sequences are susceptible to extensive homoplasy, especially for deep divergences in the Tree of Life. Retroelement insertions have emerged as a powerful alternative to sequences for deciphering evolutionary relationships because these data are nearly homoplasy-free. In addition, retroelement insertions satisfy the "no intralocus-recombination" assumption of summary coalescent methods because they are singular events and better approximate neutrality relative to DNA loci commonly sampled in phylogenomic studies. Retroelements have traditionally been analyzed with parsimony, distance, and network methods. Here, we analyze retroelement data sets for vertebrate clades (Placentalia, Laurasiatheria, Balaenopteroidea, Palaeognathae) with 2 ILS-aware methods that operate by extracting, weighting, and then assembling unrooted quartets into a species tree. The first approach constructs a species tree from retroelement bipartitions with ASTRAL, and the second method is based on split-decomposition with parsimony. We also develop a Quartet-Asymmetry test to detect hybridization using retroelements. Both ILS-aware methods recovered the same species-tree topology for each data set. The ASTRAL species trees for Laurasiatheria have consecutive short branch lengths in the anomaly zone whereas Palaeognathae is outside of this zone. For the Balaenopteroidea data set, which includes rorquals (Balaenopteridae) and gray whale (Eschrichtiidae), both ILS-aware methods resolved balaeonopterids as paraphyletic. Application of the Quartet-Asymmetry test to this data set detected 19 different quartets of species for which historical introgression may be inferred. Evidence for introgression was not detected in the other data sets.

Subject areas: Molecular systematics and phylogenetics
Key words: baleen whale, hybridization, incomplete lineage sorting, Palaeognathae, retroelements, species tree

Retroelements are a broad class of "copy-and-paste" transposable elements that comprise ~90% of the 3 million transposable elements in the human genome (Deininger and Batzer 2002; Bannert and Kurth 2004). Retroelement transposition occurs through an RNA intermediate and requires reverse transcriptase (Lander et al. 2001; Deininger and Batzer 2002). The 2 major groups of retroelements are defined by the presence/absence of long-terminal repeats (LTRs). Non-LTR retroelements include short interspersed nuclear elements (SINEs) and long interspersed nuclear elements (LINEs), which together are sometimes referred to as retroposons (Churakov et al. 2009; Nishihara et al. 2009). Processed pseudogenes comprise an additional category of non-LTR retroelements. LTR retroelements include LTR-retrotransposons and endogenous retroviruses. Endogenous viruses contain an envelope protein gene that is not a component of LTR-retrotransposons (Lander et al. 2001; Johnson 2019).

In the last 2 decades, retroelement insertions have emerged as powerful markers for resolving phylogenetic relationships (Shimamura et al. 1997; Shedlock and Okada 2000; Nikaido et al. 2001; Ray et al. 2006; Nilsson et al. 2010, 2012; Hartig et al. 2013; Doronina et al. 2015, 2017a, 2017b, 2019; Cloutier et al. 2019). In part, this is because retroelement insertions have exceptionally low levels of homoplasy relative to nucleotide substitutions in sequence-based analyses (Shedlock et al. 2000, 2004; Ray et al. 2006; Hallström et al. 2011; Kuritzin et al. 2016; Doronina et al. 2017b, 2019; Gatesy et al. 2017). The basic mechanics of the copy-and-paste process that generates retroelement insertions across the genome contrasts with the process that yields high homoplasy in DNA sequence data. In the former, new retroelement insertions almost always occur at unique genomic locations and only rarely undergo precise excision. In the case of DNA sequences, superimposed substitutions at single sites commonly flip to and fro between just 4 states (G, A, T, C), especially for deep divergences in the Tree of Life.

Conflicting retroelements that support different topologies are generally interpreted as the products of incomplete lineage sorting (ILS) rather than homoplasy when these systematic characters are properly coded (Robinson et al. 2008; Suh et al. 2011; Kuritzin et al. 2016). (See Supplementary Text for additional discussion of the practical considerations and limitations of retroelement insertions.) Avise and Robinson (2008) suggested the term hemiplasy for outcomes of ILS that mimic homoplasy. As is the case for any new mutation, a retroelement insertion is polymorphic when it first appears in a population (e.g., Lammers et al. 2019) as is required for any marker that is subject to ILS. Indeed, ILS-related problems with species tree estimation, such as the occurrence of anomalous gene trees, are not limited to sequence-based gene trees and broadly apply to other genealogical traits including genomic rearrangements and retroelement insertions (Degnan and Rosenberg 2006; Degnan J, personal communication). The possibility of an anomaly zone (Degnan and Rosenberg 2006) situation for retroelement insertions suggests that these insertions should be analyzed with ILS-aware methods that mitigate this potential problem.

Retroelement insertions have traditionally been analyzed using one or more variants of parsimony [e.g., Camin-Sokal parsimony (Nikaido et al. 1999); polymorphism parsimony (Suh et al. 2015); Dollo parsimony (Lammers et al. 2019)], distance methods [e.g., neighbor joining (Lammers et al. 2019)], and networks (e.g., Doronina et al. 2017a; Lammers et al. 2019). In particular, recent network-based analyses (Doronina et al. 2017a; Lammers et al. 2019) have used statistical methods (Huson et al. 2005; Huson and Bryant 2006) that allow for both lineage sorting and hybridization and represent a promising direction of research. In this study, we explore the use of ILS-aware methods, specifically *quartet-based methods*, to estimate species trees from retroelement insertions. We argue that species tree estimation with retroelement insertions avoids some of the practical challenges that impact gene tree summary and single-site coalescent methods.

Summary coalescent methods, such as MP-EST (Liu et al. 2010) and ASTRAL (Mirarab and Warnow 2015), operate by estimating gene trees from orthologous, recombination-free regions of the genome and then inferring a species tree from the gene trees using summary statistics. ASTRAL, for example, will identify the unrooted species trees on 4 leaves (e.g., species) from the most frequent unrooted gene tree on 4 leaves, where gene trees are assumed to evolve within a species tree under the multispecies coalescent (MSC) model (Allman et al. 2011; Degnan 2013). In particular, ASTRAL searches for a tree that maximizes the number of quartets induced by the input gene trees. ASTRAL searches with the exact option (-x) are guaranteed to find the globally optimal tree or one of the optimal trees if there are multiple trees.

ASTRAL and other summary coalescent methods assume that ILS is the only source of topological gene tree heterogeneity. However, gene tree reconstruction error can be a major source of conflict for summary coalescent analyses with sequence-based gene trees (Huang et al. 2010; Meredith et al. 2011; Patel et al. 2013; Gatesy and Springer 2014; Springer and Gatesy 2016; Scornavacca and Galtier 2017). By contrast, very low levels of homoplasy effectively liberate retroelement insertions from gene tree reconstruction error (Shedlock and Okada 2000; Shedlock et al. 2004; Ray et al. 2006; Hallström et al. 2011; Doronina et al. 2017b, 2019). This is because retroelement insertion at a specific genomic location is a rare event, as is the precise excision of an inserted sequence (Shedlock and Okada 2000; Doronina et al. 2019). Second, the basic units of analysis for a summary coalescent method are coalescence genes (c-genes), segments of the genome for which there has been no recombination over the phylogenetic history of a clade (Hudson 1990; Doyle 1992, 1997). Summary coalescent methods assume that there has been free recombination between c-genes but no recombination within c-genes. This assumption is routinely violated when complete protein-coding sequences or other long segments of the genome are assumed to be c-genes (Gatesy and Springer, 2013; Springer and Gatesy 2016, 2018a; Scornavacca and Galtier 2017; Mendes et al. 2019). C-genes become even shorter as more taxa are added to a phylogenetic analysis because of the "recombination ratchet" (Gatesy and Springer 2014; Springer and Gatesy 2016, 2018a). By contrast, the presence/absence of a retroelement is almost always due to a single mutational event (Doronina et al. 2019) and is not subject to intralocus recombination that distorts interpretation. Hence, the singularity of each retroelement insertion nullifies problems that are derived from the recombination ratchet. Unequal recombination can result in the complete deletion or duplication of a retroelement, or in a chimaeric retroelement where the 5′ and 3′ fragments are from different retroelements, but if retroelement insertions are properly coded these rare events can be detected and culled from a data set. Third, retroelements are thought to be largely neutral markers (Kuritzin et al. 2016; Chuong et al. 2017; Kubiak and Makalowska 2017; Doronina et al. 2019) as is assumed by summary coalescent methods (Liu et al. 2009). More specifically, the overwhelming majority of retroelement insertions are found in regions of the genome where they have no known functional or selective significance (Kuritzin et al. 2016; Chuong et al. 2017). There are exceptions, for

example, when retroelements provide new promoter sequences for a nearby gene (Dekel et al. 2015), but in general retroelements occur in genomic "safe havens" where they are tolerated (Chuong et al. 2017).

Beyond summary coalescent methods that employ gene trees, single-site coalescent methods such as SNAPP (Bryant et al. 2012) and SVDquartets (Chifman and Kubatko 2014) can be used to estimate a species tree from unlinked SNP data. The first step in SVDquartets consists of inferring species trees on all possible sets of 4 taxa. Importantly, the unrooted species tree on 4 taxa is identifiable using the inference method proposed by Chifman and Kubatko (2014) when certain model assumptions are met: each site is assumed to have its own genealogy under the MSC model, sequences evolve according to a molecular clock, and sites evolve down each gene tree under a single model of sequence evolution (general time-reversible [GTR] or Jukes-Cantor [JC]) (Chifman and Kubatko 2015). In the second step, quartet puzzling is used to assemble a species tree. An improved version of SVDquartets is available in PAUP* (Swofford 2002). This version of SVDquartets, which has been called SVDquartets + PAUP (Vachaspati and Warnow 2018a), uses the same procedure as the original SVDquartets method to evaluate quartets, but then assembles these quartets with the Quartet Fiduccia Mattheyses (QFM) algorithm (Reaz et al. 2014) instead of quartet puzzling. Subsequently, Vachaspati and Warnow (2018a) developed SVDquest, which uses PAUP* to choose the best quartets and dynamic programming in ASTRAL to assemble these quartets into a species tree.

Single-site methods bypass the problem of gene tree estimation error that afflicts summary coalescent analyses with sequence-based gene trees (Chou et al. 2015). Nevertheless, there can still be violations in model assumptions. For example, that sequence evolution satisfies a molecular clock (Chifman and Kubatko 2015; Abo et al. 2017) and that DNA sequence evolution for each genealogically independent site in the genome is governed by a single substitution rate matrix (Chifman and Kubatko 2015). The latter is related to violations in model assumptions that are common across standard models of DNA sequence evolution (e.g., stationarity, homogeneity, and reversibility). The DNA sequence SNPs that are input into SVDquartets are increasingly impacted by homoplasy and long branches at deeper divergences. Problems with long branches are magnified when there is poor taxon sampling, which is typically the case for quartets of taxa that are generated by subsampling a data matrix with numerous taxa. By contrast, dense taxon sampling enables subdivision of long branches and dispersion of homoplasy (properly "local synapomorphies"; Wenzel and Siddall 1999) across the tree (Hillis 1996; Graybeal 1998). Indeed, some early molecular studies on placental mammal phylogeny had poor taxon sampling and recovered murid rodents or hedgehogs as the earliest offshoots of the placental tree (e.g., Graur et al. 1991; D'Erchia et al. 1996). However, these long-branch misplacement problems have vanished with improved taxon sampling (Murphy et al. 2001; Meredith et al. 2011). Unlike DNA sequences, for which individual quartets are susceptible to problems with homoplasy on long branches, individual retroelement insertions remain virtually homoplasy-free even at deep phylogenetic nodes and should not suffer from this problem (Waddell et al. 2001). Finally, the assumption of free recombination among sites is violated when SNP methods are applied to multiple linked sites in a gene. By contrast, retroelement insertions almost always occur at dispersed sites.

In summary, retroelements avoid many of the practical challenges of estimating species trees from inferred gene trees or unlinked SNPs. Therefore, the analysis of retroelement data sets using ILS-aware methods may greatly improve species tree estimation in the presence of rapid radiations at deep divergences.

Retroelement insertions, like DNA sequences, are also relevant for assessing whether introgression has occurred in the evolutionary history of a clade. Conflicting phylogenetic distributions of biallelic DNA sequence markers are routinely analyzed with the ABBA-BABA test, which uses the D statistic (Green et al. 2010). This test was originally developed to assess SNP data for evidence of gene flow between 1 of 2 human populations and Neandertals and assumed that the primitive state for each SNP occurred in the chimpanzee outgroup (Green et al. 2010). More recently, a similar statistical test, named KKSC after the last names of the 4 authors, was developed for inferring introgression based on the distribution of conflicting retroelements among 3 ingroup taxa relative to an outgroup that lacks the insertions (Kuritzin et al. 2016). Both the ABBA-BABA and KKSC tests can be used to determine whether ILS alone can explain the distribution of conflicting patterns among 3 ingroup species. These tests consider cases where a SNP or retroelement insertion originates in the ancestor of 2 or 3 ingroup taxa (Figure 1A–D), but do not consider cases where a SNP or retroelement insertion originates in the common ancestor of all 4 taxa and then undergoes lineage sorting (Figure 1E–H). Importantly, the latter scenario will result in 0011 and 1100 patterns that are both consistent with the quartet split WX|YZ (Figure 1E–H). A more general test than the ABBA-BABA test or KKSC test would account for all of the patterns that result from a SNP or retroelement insertion in the ancestor all 4 lineages, and would also allow for the analysis of symmetrical quartets of taxa in a larger species tree.

Here, we develop 2 quartet-based, ILS-aware methods (Figure 2) for species tree construction and apply these methods to 5 retroelement data sets (Nishihara et al. 2009 [Placentalia]; Doronina et al. 2017a [Laurasiatheria-102, Laurasiatheria-139]; Cloutier et al. 2019 [Palaeognathae]; Lammers et al. 2019 [Balaenopteroidea]). Both of these methods are motivated by the identifiability of the unrooted species tree on 4 species from the most probable unrooted 4-taxon gene tree, with the 2 alternative (gene tree) quartets having equal probability (Allman et al. 2011; Degnan 2013). We expect the same relationship between retroelements supporting different quartet topologies under ILS with random mating (Slatkin and Pollack 2008) unless there is also introgression or lateral transfer of genomic material (Kuritzin et al. 2016). Then, we propose a Quartet-Asymmetry test (Figure 3) that is similar to the ABBA-BABA (Green et al. 2010) and KKSC (Kuritzin et al. 2016) tests for 3 ingroup taxa. The Quartet-Asymmetry test does not require an outgroup, enabling the analysis of all 4-taxon unrooted subtrees independent of whether the rooted versions of these trees are pectinate or symmetric in the overall species tree. Because retroelement insertions are low-homoplasy characters, even for species trees with relatively ancient divergences and short internodes, we argue for the utility of this approach for discriminating between ILS alone versus ILS + introgression for lineages that diverged as deep as the Upper Cretaceous. By contrast, the application of analogous ABBA-BABA tests (Green et al. 2010) to DNA sequences at this depth is challenged by superimposed substitutions at the same nucleotide position (convergence, parallelism, reversal, and other multiple hits), lineage-specific rate variation, and model misspecification. We apply the Quartet-Asymmetry test to all 5 data sets, 4 of which encompass divergences that extend into the Cretaceous (Meredith et al. 2011; dos Reis et al. 2012; Jarvis et al. 2014).

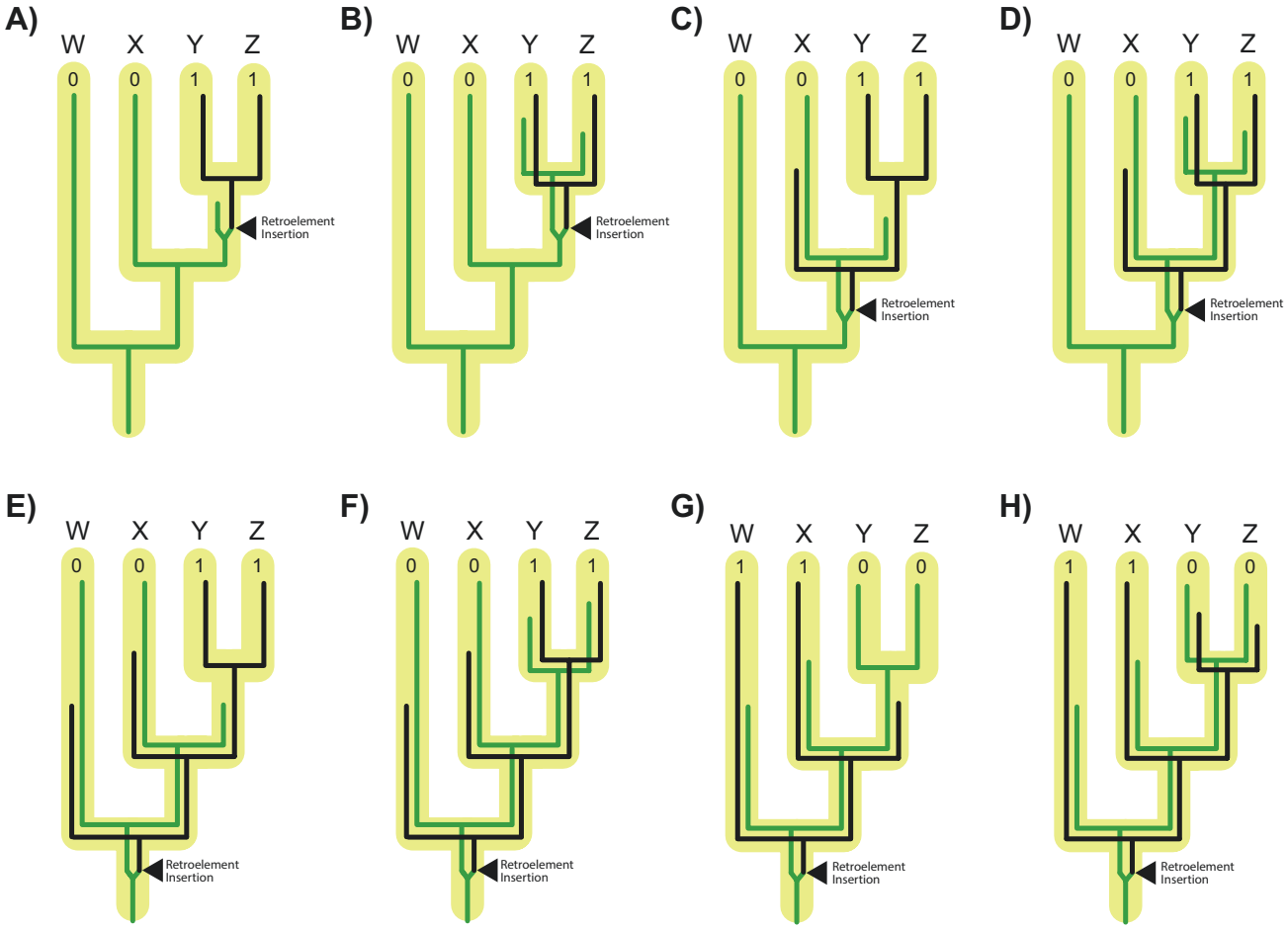

Figure 1. Schematic of different scenarios that will result in 0011 and 1100 retroelement insertion patterns. These scenarios include synapomorphic changes, changes that mimic synapomorphy, and outcomes of lineage sorting that result in the presence of a retroelement insertion in nonsister taxa. In **A**, a synapomorphic retroelement originates in the common ancestral lineage of Y and Z and is fixed in the common ancestral lineage of Y and Z, resulting in a 0011 pattern. In **B**, a synapomorphic retroelement originates in the common ancestral lineage of Y and Z but is fixed independently in Y and Z, resulting in a 0011 pattern. In **C** and **D**, a retroelement insertion originates in the common ancestral lineage of X, Y, and Z. In **C**, the retroelement is lost in X and fixed in the common ancestral lineage of Y and Z. In **D**, the retroelement is lost in X and fixed independently in Y and Z. In both **C** and **D**, the 0011 pattern mimics synapomorphy because the retroelement insertion is present in sister taxa Y and Z, but did not originate in the most recent common ancestor of Y and Z and instead is the result of lineage sorting. In **E**–**H**, a retroelement insertion originates in the common ancestral lineage of all 4 taxa (W, X, Y, Z) and results in either a 0011 pattern (**E**, **F**) or 1100 pattern (**G**, **H**) through lineage sorting. The 0011 pattern (**E**, **F**) mimics synapomorphy, but the insertion that is present in sister taxa Y and Z did not originate in the immediate common ancestral lineage of Y and Z and instead is the result of lineage sorting. In the 1100 pattern (**G**, **H**), the presence of the retroelement insertion in nonsister taxa W and X is the result of lineage sorting. Likewise, the absence of the retroelement in sister taxa Y and Z is the result of lineage sorting.

Methods

Retroelement Data Sets

The first data set (Placentalia) is comprised of 68 LINE insertions that are informative for resolving relationships among 3 major clades of placental mammals (Afrotheria [e.g., elephants, hyraxes, tenrecs], Boreoeutheria [e.g., primates, rodents, bats], Xenarthra [e.g., anteaters, sloths, armadillos]) that diverged from each other at the base of this clade (Nishihara et al. 2009). Retroelement counts for the 3 different resolutions of Placentalia are 22 for Boreoeutheria + Xenarthra, 25 for Afrotheria + Boreoeutheria, and 21 for Afrotheria + Xenarthra. Each of the 3 ingroup taxa (Afrotheria, Boreoeutheria, Xenarthra) in the data set is coded as absent (0) or present (1) for each retroelement character (i.e., there are no missing data), and the outgroup is coded as absent for all 68 characters. Previously, Nishihara et al. (2009) concluded that these 3 lineages diverged from each other nearly simultaneously in the Cretaceous.

The second data set (Laurasiatheria-102) is comprised of 102 retroelements (76 LINEs, 23 LTRs, and 3 retropseudogenes) for 4 orders of Laurasiatheria (Carnivora [e.g., dogs, cats], Cetartiodactyla [e.g., pigs, cows, whales], Chiroptera [bats], Perissodactyla [e.g., horses, rhinos]) and the outgroup Eulipotyphla (e.g., shrews, moles, hedgehogs) (Doronina et al. 2017a). For this data set, retroelement insertions support ten different bipartitions that are phylogenetically informative for resolving ingroup relationships. Retroelement counts for the Laurasiatheria data set range from 4 to 14 for different bipartitions of taxa and were scored using Doronina et al.'s (2017a) figure 1. There are no missing data for these 102 retroelement insertions. We also analyzed an expanded data set from Doronina et al. (2017a) that included an additional order of Laurasiatheria (Philodota [pangolins]) and 162 retroelements. Some of the additional retroelements were scored as missing for the eulipotyphlan outgroup, and others show distribution patterns that conflict with the monophyly of Scrotifera (all laurasiatherians excepting

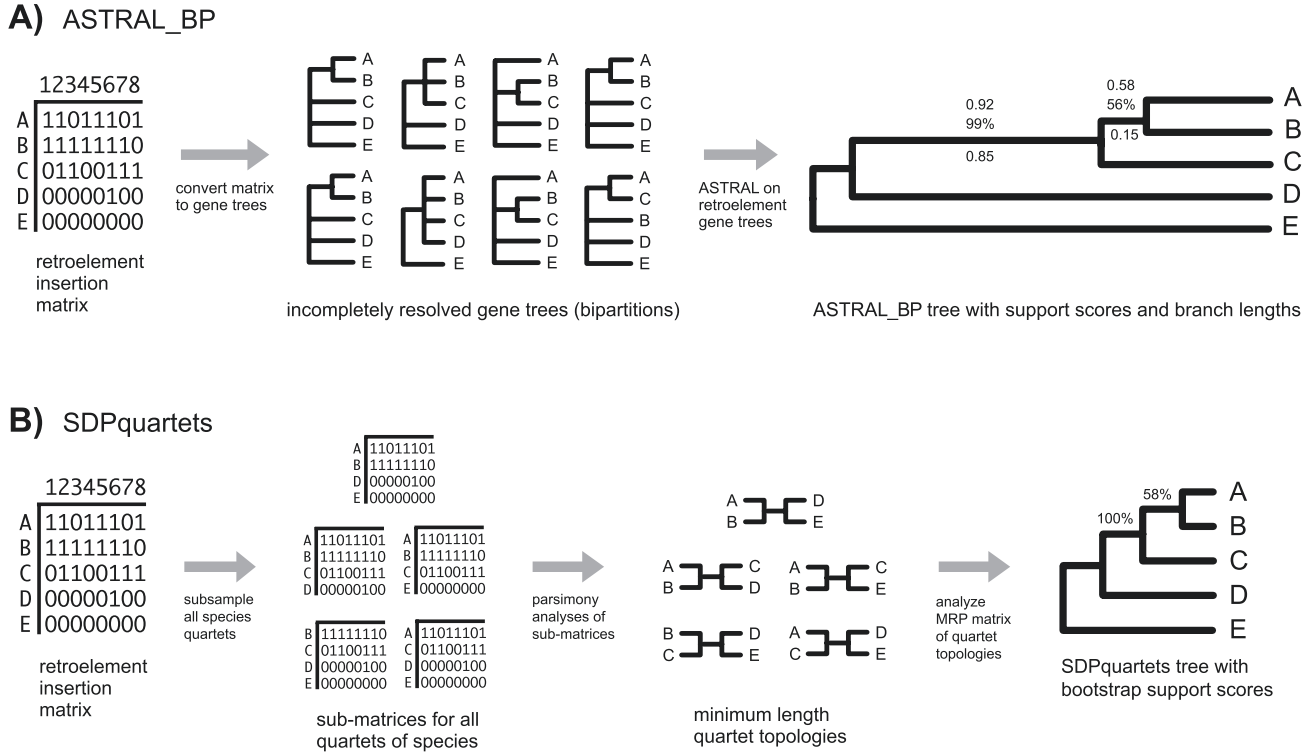

Figure 2. Schematic of 2 ILS-aware methods that can be used to reconstruct a species tree from a retroelement insertion matrix: (**A**) In ASTRAL_BP, ASTRAL is used to analyze gene trees, each of which includes just one bipartition of taxa for each retroelement insertion character, and (**B**) in SDPquartets, parsimony analyses of all retroelement insertion characters are executed for all possible quartets of species, and optimal quartet trees are analyzed in ASTRAL or using parsimony analysis of an MRP supertree matrix derived from the optimal quartet trees. Taxon E is the user-specified outgroup. In **A**, estimated branch lengths in coalescent units are indicated below 2 internal branches, and Bayesian local posterior probabilities and bootstrap support percentages are above internal branches. In **B**, bootstrap percentages are above internal branches. Note that sample sizes for estimation of topology, support scores, and branch lengths are small in this simple contrived example.

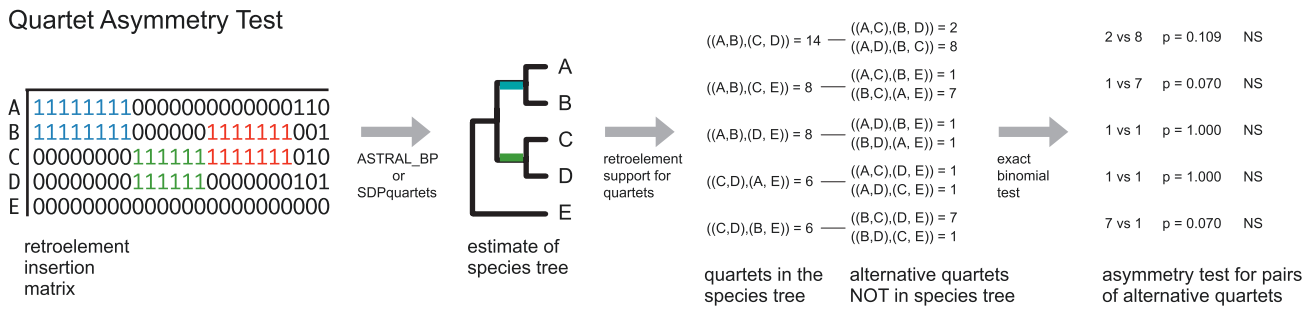

Figure 3. Schematic showing Quartet-Asymmetry tests for a retroelement matrix. The first step is to construct a species tree using ASTRAL_BP or SDPquartets (Figure 2). Next, every combination of 4 species is examined individually to test if the 2 alternative quartets that are not in the species tree are equally supported by retroelement insertions as expected under ILS. A χ^2 or binomial test with a correction for multiple tests is used to assess statistical significance. Quartets of species with significant differences in the number of alternative quartets provide evidence for introgression pathways. Note that in this hypothetical case, none of the 3 quartets show significant asymmetry based on the exact binomial test so it was not necessary to perform a correction for multiple tests. Retroelements that support clade A + B are colored blue, retroelements that support clade C + D are colored green, and retroelements that support the conflicting clade B + C are colored red. Additional retroelements that conflict with the species tree (last 3 columns in the matrix) are in black and are not highlighted.

Eulipotyphla). Also, only 139 of these retroelements are informative for resolving unrooted quartets of taxa. We subsequently refer to this data set as Lauraiatheria-139.

The fourth retroelement data set (Balaenopteroidea) is based on a genome-wide scan that identified 24 598 CHR2-SINE insertions for balaenopteroid baleen whales (Lammers et al. 2019). These SINE insertions occur in 2 or more of 6 balaenopteroid species, but not in the outgroup Balaenidae. Of the 24 598 CHR2-SINE insertions, 17 225 are informative for resolving relationships among the 6 balaenopteroids, which include 5 balaenopterids (*Balaenoptera acutorostrata* [common minke whale], *Balaenoptera musculus* [blue whale], *Balaenoptera borealis* [sei whale], *Balaenoptera physalus* [fin whale], *Megaptera novaeangliae* [humpback whale]) and one eschrichtiid (*Eschrichtius robustus* [gray whale]). The balaenid outgroup is *Eubalaena glacialis* [North Atlantic right whale]). This data set consists of 57 different bipartitions with counts that range from 46 to 7373 (Supplementary Table S1). There are no missing data in the balaenopteroid data set.

The final retroelement data set (Palaeognathae) is from Cloutier et al. (2019; also see Sackton et al. 2019) and is comprised of 4301 retroelement insertions found in Palaeognathae (ratites and tinamous). These retroelement insertions were scored for 12 ingroup species and a single outgroup (chicken) and provide support for 20 different bipartitions of taxa with counts that range from 1 to 2318. Retroelement distributions for Palaeognathae were taken from Cloutier et al.'s (2019) online file ("CR1_insertion_pattern_summary.xls") and used to construct a presence/absence matrix (i.e., 01 matrix). Retroelement insertions that were scored as missing (M) or omitted (O) by Cloutier et al. (2019) were scored as missing (?) in our 01 retroelement insertion matrix. This matrix was then converted into a file with 4301 Newick bipartitions (see below).

Species Tree Estimation Using Retroelement Insertions

Here, we present 2 different methods for estimating species trees from retroelement insertions in the presence of ILS. Both approaches operate by weighting each quartet of species based on the number of retroelement insertions that support that quartet and then assembling the weighted quartets into a tree on the full set of species.

Our first approach, ASTRAL with bipartitions (ASTRAL_BP), effectively weights each possible quartet tree by its frequency in the retrolement insertion matrix, and then assembles the weighted quartets using ASTRAL. Our second approach uses split decomposition with parsimony (SDP) followed by quartet assembly and is referred to as SDPquartets. This method infers unrooted species trees on sets of 4 taxa by examining the number of retroelement insertions that support each of the 3 possible quartet topologies. Importantly, under ILS with neutrality and panmixia there is no anomaly zone for the unrooted 4-taxon species tree. Therefore, the most probable unrooted gene tree on 4 species agrees with the unrooted species tree on 4 species, with the 2 alternative (gene tree) quartets having equal probability (Degnan and Rosenberg 2009; Ané 2010; Allman et al. 2011; Degnan 2013). We expect a similar relationship for retroelement insertions if a constant rate of retroelement insertion per generation, neutrality, and panmixia are assumed.

ASTRAL_BP

For ASTRAL_BP (Figure 2A), the first step is to convert each matrix of presence/absence characters into a set of incompletely resolved "gene trees" with each gene tree representing a single retroelement character and supporting just a single bipartition of taxa. We used a custom script (https://github.com/ekmolloy/phylotools) to convert a presence/absence matrix of retroelement insertions (phylip format) into a file with one Newick string per retroelement insertion. Taxa that were scored as missing (?) for a given retroelement were excluded from the corresponding Newick string (only the Palaeognathae and Laurasiatheria-139 data sets had missing data). We then executed ASTRAL-II v. 4.11 (Mirarab and Warnow 2015) given the incompletely resolved "gene trees" as input (Figure 2A). When run in this fashion, ASTRAL computes the frequency with which each quartet appears in the retroelement insertion matrix and then solves the maximum quartet support supertree (MQSS) problem exactly within a constrained search space that includes all bipartitions defined by retroelement insertions. Because the data sets analyzed in this study had sufficiently small numbers of taxa, we were able to run ASTRAL in "exact" mode (-x), meaning that every possible bipartition is included in the search space. Thus, the species tree returned by ASTRAL is a global optimum for the MQSS problem. A caveat is that ASTRAL will only find one optimal tree even if there are multiple optimal trees (Vachaspati and Warnow 2018b). This caveat applies to all analyses that are run with current implementations of ASTRAL including analyses with sequence-based gene trees.

The output of ASTRAL includes the inferred species tree, estimated branch lengths in coalescent units (CUs), and local posterior probabilities (PPs) for each supported clade (Sayyari and Mirarab 2016). Bootstrapping with 1000 pseudoreplicates in ASTRAL provided a second measure of clade support. Simmons et al. (2019) argued that gene-wise bootstrap resampling is more appropriate than site-wise bootstrap resampling for summary coalescent analyses, but for bipartitions that represent single retroelement insertions, these 2 support measures are effectively identical. Finally, we tested the stability of supported clades in a third way by estimating the minimum number of gene tree removals that are required to collapse each clade (Gatesy et al. 2017, 2019) using ASTRAL v. 5.6.3.

ASTRAL is typically applied to fully resolved gene trees, but both ASTRAL-II (Mirarab and Warnow 2015) and ASTRAL-III (Zhang et al. 2017, 2018) accept gene trees with polytomies. When a branch in a gene tree is collapsed (creating a polytomy), the corresponding bipartition and the quartets induced by only that bipartition are removed from the gene tree. Thus, polytomies have the potential to impact ASTRAL by changing the quartet frequencies and the constrained search space; the latter issue is only problematic when ASTRAL cannot be run in exact mode, and thus does not impact the results of our study. Of course, gene tree estimation error also changes the quartet frequencies and the constrained search space. Zhang et al. (2018) advocated highly conservative filtering of internal branches on gene trees that are not well supported. This strategy has been employed in analyses with both sequence-based gene trees (Blom et al. 2017; Longo et al. 2017; Chen et al. 2019) and indel-based gene trees (Houde et al. 2019). For example, Houde et al. (2019) collapsed more than 60% of the internal branches in some of their indel-based gene trees that were analyzed with ASTRAL. A similar collapsing of very short branches in gene trees is also the default option of the summary coalescent method MP-EST 2.0 (Liu et al. 2010).

Our implementation of ASTRAL with retroelement bipartitions, ASTRAL_BP, could be viewed as an extreme variant of collapsing clades because each gene tree includes only a single bipartition. Nevertheless, these bipartitions presumably have higher accuracy than bipartitions on sequence-based gene trees because independent retroelement insertions at the exact same genomic site (convergence) are rare and the probability of precise excision of a retroelement (reversal) is extremely small (Doronina et al. 2019). As noted by Zhang et al. (2018), future work should examine conditions where ASTRAL remains statistically consistent in challenging regions of tree space, such as the anomaly zone, when poorly supported branches on sequence-based gene trees are collapsed. Similar studies should examine the limiting case of single bipartitions that have high reconstruction accuracy (e.g., retroelement insertions).

SDPquartets

SDPquartets, like other split decomposition methods, consists of 2 discrete steps that are performed in series: 1) parsimony analysis of all possible species quartets in the 01 retroelement matrix and 2) subsequent assembly of the most parsimonious quartets into a species tree that fits the most quartets (Figure 2B). For step 1, we note that the most parsimonious quartet is equivalent to the most

frequent quartet, and thus parsimony is well-suited for the inference of unrooted quartets with retroelements. For step 2, we used matrix representation with parsimony (MRP) (Ragan 1992). The logic here is that the most parsimonious tree(s) based on the MRP matrix is one and the same as the tree(s) that is compatible with the maximum number of quartets. This is because each quartet that fits a given species tree perfectly will have just one step, but if the quartet does not fit that species tree, 2 steps will be required. Therefore, minimizing the number of steps also maximizes the fit of quartets to alternative species tree topologies. Quartet assembly could also be performed using other supertree methods as well as methods that are explicitly designed for quartets, including ASTRAL, as is the case for SVDquest (Vachaspati and Warnow 2018a), Quartet Max Cut (Snir and Rao, 2012), or QFM (Reaz et al. 2014). Importantly, the MQSS problem is an NP-hard optimization problem (Jiang et al. 2000), and thus all of these approaches (except ASTRAL run in exact mode or MRP run in exact [branch-and-bound] or exhaustive mode) are heuristics, that is, they are not guaranteed to return a tree with maximal quartet support.

SDPquartets was implemented in a custom Perl script (https://github.com/dbsloan/SDPquartets). In the first step (quartet inference), the script directs PAUP* (Swofford 2002) to evaluate all possible quartets and save the most parsimonious tree(s) for each quartet of species to a treefile. The script also implements nonparametric bootstrapping of the original retroelement matrix by resampling characters with replacement. We employed this script to generate 1000 bootstrap pseudoreplicates for each data set that we analyzed with SDPquartets. To address the possibility of equally parsimonious ties for a given quartet of species, we employed 6× weighting for a quartet tree that is the single most parsimonious resolution for a quartet of species, 3× weighting for the best trees when there are 2 equally most-parsimonious trees, and 2× weighting when all 3 trees for a quartet of species are equally parsimonious. This weighting was accomplished by writing the most parsimonious tree(s) to the treefile 6 times, 3 times, or 2 times, as appropriate. In the second step (quartet assembly), the script employs the MRP (Ragan 1992) option in PAUP* to convert the most parsimonious species quartets in the treefile into a 01 MRP matrix. For parsimony searches with the MRP matrices for both the original data sets and the bootstrap resamplings, we used the branch and bound (bandb) search option to ensure identification of multiple parsimonious trees. For each SDPquartets bootstrap pseudoreplicate, if there were multiple most parsimonious trees in the MRP matrix search, a strict consensus was constructed before inclusion in an extended majority rule consensus of all 1000 bootstrap pseudreplicates. Analyses were performed with the current Linux command-line version of PAUP* (paup4a166_centos64).

Quartet-Asymmetry Test for Introgression

The expectation under ILS without hybridization is that the number of retroelement characters that support each of the 2 nonspecies-tree quartets will be equal (Degnan and Rosenberg 2009; Ané 2010). By contrast, introgression has the potential to distort this 50:50 ratio, with one alternative quartet tree overrepresented relative to the second alternative quartet tree. To determine if ILS alone can explain the distribution of conflicting quartets, we propose a general Quartet-Asymmetry test that is similar to the ABBA-BABA test (Green et al. 2010) for DNA sequences and the KKSC test (Kuritzin et al. 2016) for retroelement insertions. The ABBA-BABA and KKSC tests only count patterns where the outgroup lacks the derived state (i.e., 0011 [AA|BB], 0110 [AB|BA], and 0101 [BA|BA]) and thus do not count the other 3 phylogenetically informative patterns: 1100 (corresponding to AA|BB), 1001 (corresponding to AB|BA), and 1010 (corresponding to BA|BA). Importantly, all 6 of these patterns are possible when the derived state (e.g., a retroelement insertion) originates in the ancestral population of all 4 species. By counting these patterns, our proposed general Quartet-Asymmetry test can be applied to unrooted 4-taxon species tree topologies to determine whether ILS alone explains the distribution of conflicting patterns. However, unlike the KKSC test, the Quartet-Asymmetry test merely tests for evidence of introgression and does not provide statistical support for any particular network topology, and inferring phylogenetic networks on 4 species can be quite challenging when there is ILS (Yu et al. 2011).

The Quartet-Asymmetry test can be performed with a χ^2 statistic or a binomial distribution (e.g., exact binomial test using binom.test function in R) if there are concerns with sample size. The minimum number of retroelement insertions for conflicting topologies that is required to obtain a significant result with the exact binomial test is 6. The Quartet-Asymmetry test can be applied to both symmetric and pectinate 4-taxon subtrees (Figure 3) and unlike the ABBA-BABA test (Green et al. 2010) and KKSC test (Kuritzin et al. 2016) allows for derived states (i.e., retroelement insertions) that originate in the common ancestor of all 4 taxa.

In the case of pectinate species trees, there are 3 different scenarios where ILS will result in ABBA and BABA patterns with equal probabilities. In the first scenario (Figure 4A and B), the retroelement insertion (state 1 = black gene lineages) originates in the common ancestor of all 4 taxa, is retained across the basal split of the species tree, and is lost by lineage sorting in W (Figure 4A and B) and in Z (Figure 4A) or Y (Figure 4B). The retroelement absence allele (state 0 = green gene lineages), in turn, is lost in X (Figure 4A and B) and in Y (Figure 4A) or Z (Figure 4B). In the second scenario (Figure 4C and D), the retroelement insertion also originates in the common ancestor of all 4 taxa. However, in this case the ABBA and BABA patterns result through lineage sorting when the retroelement insertion allele is lost in X (Figure 4C and D) and in Y (Figure 4C) or Z (Figure 4D). The retroelement absence allele, in turn, is lost in W (Figure 4C and D) and in Z (Figure 4C) or Y (Figure 4D). In the third scenario, the retroelement insertion originates in the common ancestor of X, Y, and Z (Figure 4E and F). In the ABBA pattern (Figure 4E), the retroelement insertion allele is lost in Z and the retroelement absence allele is lost in X and Y. In the BABA pattern (Figure 4F), the retroelement insertion allele is lost in Y and the retroelement absence allele is lost in X and Z.

The rationale for application of this test to symmetric subtrees (Figure 4G–J) is that each of the 2 alternative quartet trees are equally likely under the MSC, as is the case for the application of this test with pectinate subtrees of 4 taxa (Figure 4A–F). This is because the alternate quartet resolutions have equivalent amounts of time (branch lengths) on the species tree for ABBA (0110 or 1001) and BABA (1010 or 0101) patterns under ILS with neutrality and panmixia (Figure 4G–J). However, for symmetric trees the retroelement insertion must originate in the common ancestor of all 4 taxa and there are only 2 scenarios where ABBA and BABA patterns occur with equal probabilities (Figure 4G–J). In the first scenario (Figure 4G and H), the retroelement insertion allele is lost in W (Figure 4G and H) and in Z (Figure 4G) or Y (Figure 4H), and the retroelement absence allele is lost in X (Figure 4G and H) and in Y (Figure 4G) or Z (Figure 4H). In the second scenario (Figure 4I and J), the retroelement insertion allele is lost in X (Figure 4I and J) and

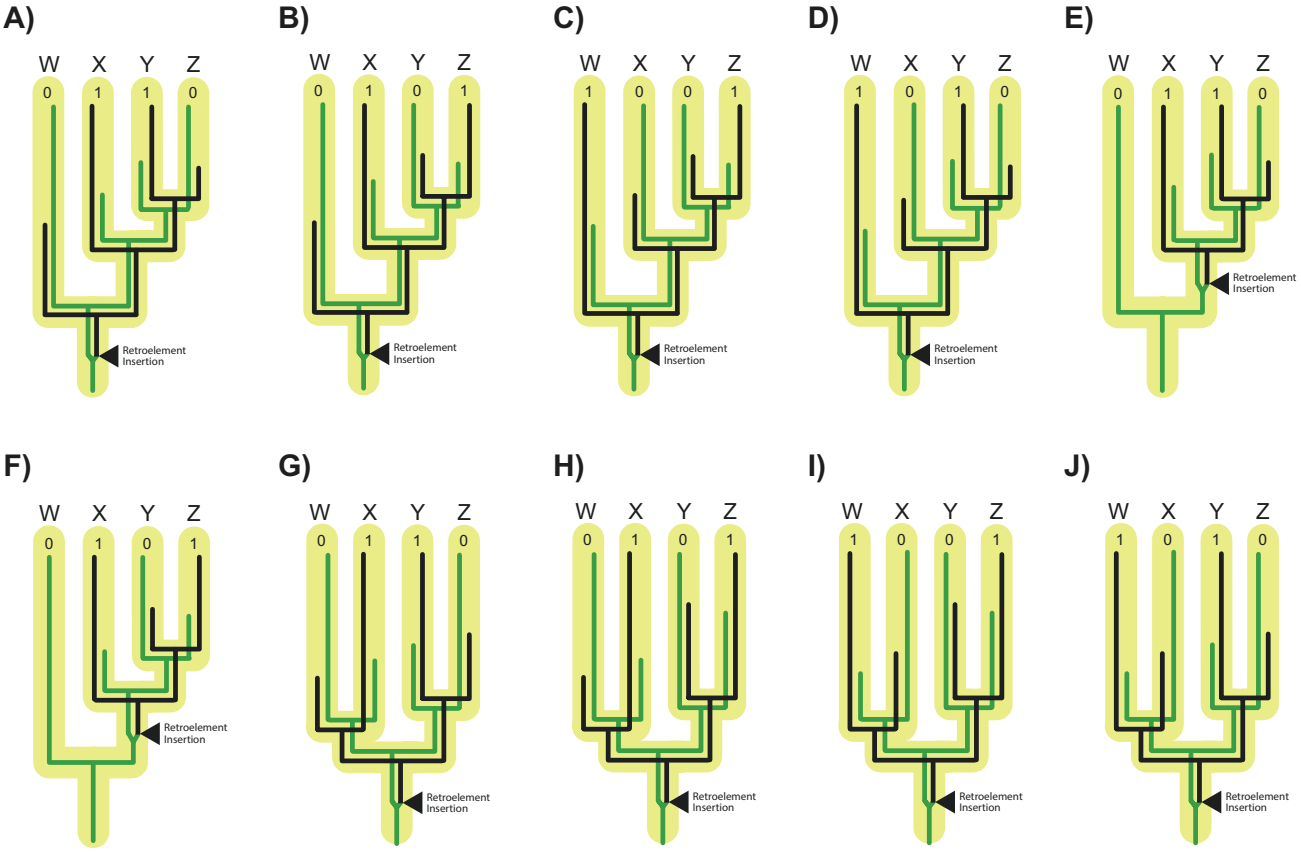

Figure 4. Illustration of ABBA-BABA patterns for the distribution of retroelement insertions on pectinate and symmetric species trees for 4 taxa (W, X, Y, Z). In all cases, the quartet split on the unrooted species tree is WX|YZ. In **A**–**F**, a pectinate species tree is associated with complementary pairs of retroelement bipartitions (**A** versus **B**, **C** versus **D**, **E** versus **F**) that disagree with the species tree and have equal probabilities for ABBA and BABA hemiplasy via ILS under neutrality and random mating. ABBA (0110 or 1001) and BABA (0101 or 1010) patterns can arise if the retroelement insertion originates in the common ancestral lineage of all 4 taxa (**A**–**D**) or in the common ancestral lineage of X, Y, and Z (**E** and **F**). **A** and **B** show equal probabilities for 0101 and 0110 patterns when the retroelement originates in the ancestor of all 4 taxa (W, X, Y, Z). Similarly, equal probabilities exist for 1010 and 1001 patterns (**C** and **D**). **E** and **F** show equal probabilities for 0110 and 0101 patterns when the retroelement originates in the ancestor of 3 taxa (X, Y, Z). Overall, ABBA and BABA patterns have equal probability. In **G**–**J**, symmetric trees have equal opportunities for ABBA and BABA hemiplasy with ILS under neutrality, but will only occur when the retroelement insertion originates in the common ancestral lineage of all 4 taxa. **G** and **H** show 0110 and 0101 patterns, respectively, that have equal probabilities. **I** and **J** show 1001 and 1010 patterns, respectively, that also have equal probabilities. Again, ABBA and BABA patterns have equal probability. Retroelement presence alleles are shown in black and retroelement absence alleles are shown in green. See main text for additional details.

in Y (Figure 4I) or Z (Figure 4J), and the retroelement absence allele is lost in W (Figure 4I and J) and in Z (Figure 4I) or Y (Figure 4J).

We applied the Quartet-Asymmetry test to each data set (Placentalia, Laurasiatheria-102, Laurasiatheria-139, Balaenopteroidea, Palaeognathae) that was included in our study. For 2 ASTRAL_BP species trees (Placentalia, Balaenopteroidea), we examined each unique quartet of species and compared the observed and expected number of retroelements that support each of the 2 quartet trees that conflict with the inferred species tree. For both Laurasiatheria data sets (Laurasiatheria-102, Laurasiatheria-139), we examined each possible quartet for the 5 core taxa (Carnivora, Cetartiodactyla, Chiroptera, Eulipotyphla, Perissodactyla). For Palaeognathae, we examined 5 quartets that sampled 5 deep lineages of Palaeognathae (ostrich, emu, Chilean tinamou, great spotted kiwi, and greater rhea). For each data set, we executed the 01 matrix (nexus format) of retroelement characters in PAUP* 4.0a165 (Swofford 2002) (Figure 3). Next, we deleted all taxa except for the 4 taxa that comprise the relevant quartet. This was accomplished with the "delete" command. Uninformative characters for each quartet were then excluded ("exclude" command) and the number of informative characters for each quartet was recorded in an Excel spreadsheet. We then performed a parsimony search for each quartet with the option to save "best trees" set to 3; these 3 trees correspond to all 3 unrooted trees for any given quartet of taxa. The number of steps for each tree was then recorded in the same Excel spreadsheet. Based on the number of informative characters for each quartet and the minimum number of steps for each quartet tree, we then calculated the number of retroelement insertions that support the quartet that is compatible with the species tree and each of the alternative conflicting quartet trees. Specifically, the number of supporting characters for each resolution of a quartet of taxa = total no. of characters – (quartet tree length – total no. of characters). These calculations were performed with an Excel calculator ("Retroposon_Introgression_Calculator.xlsx" in Supplementary Material). Because multiple quartets of species were examined in each species tree, we employed a Holm-Bonferroni sequential correction (Holm 1979) with Gaetano's (2018) EXCEL calculator to account for multiple comparisons.

Simulation of Gene Trees

Ten thousand gene trees were simulated from the ASTRAL_BP retroelement species trees for both Laurasiatheria-102 and Palaeognathae (branch lengths in CUs) using DendroPy v3.12.0 (Sukumaran and Holder 2010) and a script from Mirarab et al. (2014a). In anomaly zone conditions, the most probable gene tree does not match the species tree (Degnan and Rosenberg 2006, 2009). The simulated gene tree outputs were used to determine whether the most common gene tree topology conflicts with the species tree.

Results and Discussion

Placentalia Retroelements

The ASTRAL_BP and SDPquartets species trees for the Placentalia data set of 68 retroelement insertions both resolve the clade Afrotheria + Boreoeutheria, but with low bootstrap support (58%) and local PP (0.52) values on the ASTRAL tree (Figure 5A) and a correspondingly low PAUP* bootstrap value (54%) on the SDPquartets tree (Figure 5A). The removal of just 3 bipartitions (out of 68) collapses the clade in ASTRAL_BP analysis, further suggesting instability and low support due to extensive conflicts in the retroelement insertion data. Indeed, among the 68 retroelement insertions there are 22 that support Boreoeutheria + Xenarthra, 25 that support Afrotheria + Boreoeutheria, and 21 that support Afrotheria + Xenarthra. The internal branch length uniting Afrotheria and Boreoeutheria is very short (0.0445 CUs), especially relative to long terminal branches in the tree that extend to the Cretaceous (Figure 5B; Meredith et al. 2011). Kuritzin et al. (2016) performed the KKSC test on this same data set and concluded that there is no compelling evidence for ancient hybridization among lineages. In agreement with Kuritzin et al. (2016), we did not find any support for introgression based on the single species quartet (outgroup, Xenarthra, Afrotheria, Boreoeutheria) that we examined with the Quartet-Asymmetry test using the exact binomial test ($P = 1.0$). The mixed support that retroelements provide for different resolutions of the placental root is consistent with the conflicting results of sequence-based phylogenetic studies that favor Xenarthra + Boreoeutheria (Murphy et al. 2001; Meredith et al. 2011 [DNA], McCormack et al. 2012; Romiguier et al. 2013), Afrotheria + Boreoeutheria (Waddell et al. 2001), and Afrotheria + Xenarthra (Song et al. 2012; Meredith et al. 2011 [amino acids], Morgan et al. 2013; Tarver et al. 2016; Chen et al. 2017; Liu et al. 2017).

Laurasiatheria Retroelements

We re-examined the Laurasiatheria polytomy by analyzing both the higher stringency Laurasiatheria-102 data set (no missing data) and lower stringency Laurasiatheria-139 data set (missing data) from Doronina et al. (2017a). This polytomy is perhaps the most challenging interordinal problem in all of Placentalia given that it involves 4 lineages (Carnivora + Pholidota, Cetartiodactyla, Chiroptera, Perissodactyla) that diverged in the Late Cretaceous and 2 very short internal branches (Meredith et al. 2011; dos Reis et al. 2012; Emerling et al. 2015; Foley et al. 2016; Tarver et al. 2016). Previous investigations of this systematic problem have employed both genome-scale DNA sequence data and retroelement insertions, yielding highly incongruent results (Nishihara et al. 2006; Hallström et al. 2011; Meredith et al. 2011; Song et al. 2012; Tarver et al. 2016; Chen et al. 2017; Doronina et al. 2017a; Feijoo and Parada 2017; Liu et al. 2017). Some of these analyses are further complicated by homology problems with the underlying data (Springer and Gatesy 2016, 2017; Gatesy and Springer 2017; Springer et al. 2019). Our ASTRAL_BP and SDPquartets analyses of Doronina et al.'s (2017a) data sets recovered the same species tree reported by these authors based on polymorphism parsimony (Felsenstein 1979) (Figure 6). With the 102-retroelement data set (5 taxa), Carnivora and Cetartiodactyla are sister taxa, with Perissodactyla and Chiroptera as successively more distant relatives to this clade (Figure 6A and B). Relationships among these laurasiatherian orders are identical for the 139-retroelement data set (6 taxa), and the additional order (Phoilidota) is positioned as the sister taxon

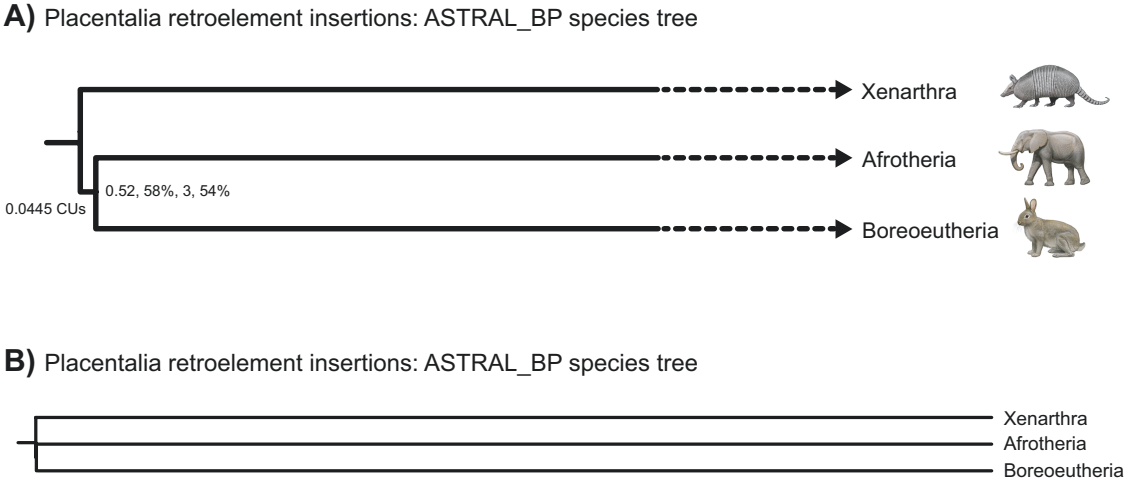

Figure 5. ASTRAL species trees for Placentalia (**A** and **B**). The first 3 numbers at the internal node correspond to local PP, ASTRAL bootstrap support percentage, and the minimum number of retroelement bipartitions that must be removed to collapse the clade in ASTRAL_BP analysis; the fourth number is the SDPquartets bootstrap percentage. Terminal branches are truncated in **A** so that the short length of the single internal branch, in coalescent units (CUs), can be seen. The species tree in **B** shows the entire terminal branch lengths in CUs, demonstrating the extreme length of terminal branch relative to the very short internal branches that is barely visible. CU estimates for terminal branches are derived from molecular clock analyses (Meredith et al. 2011) because ASTRAL does not estimate terminal branch lengths. One million years from timetree estimates were converted to one CU (see Springer and Gatesy 2016 for rationale). Relationships in the SDPquartets species tree are identical to those in the ASTRAL_BP species tree that is shown. Illustrations of mammals are by C. Buell.

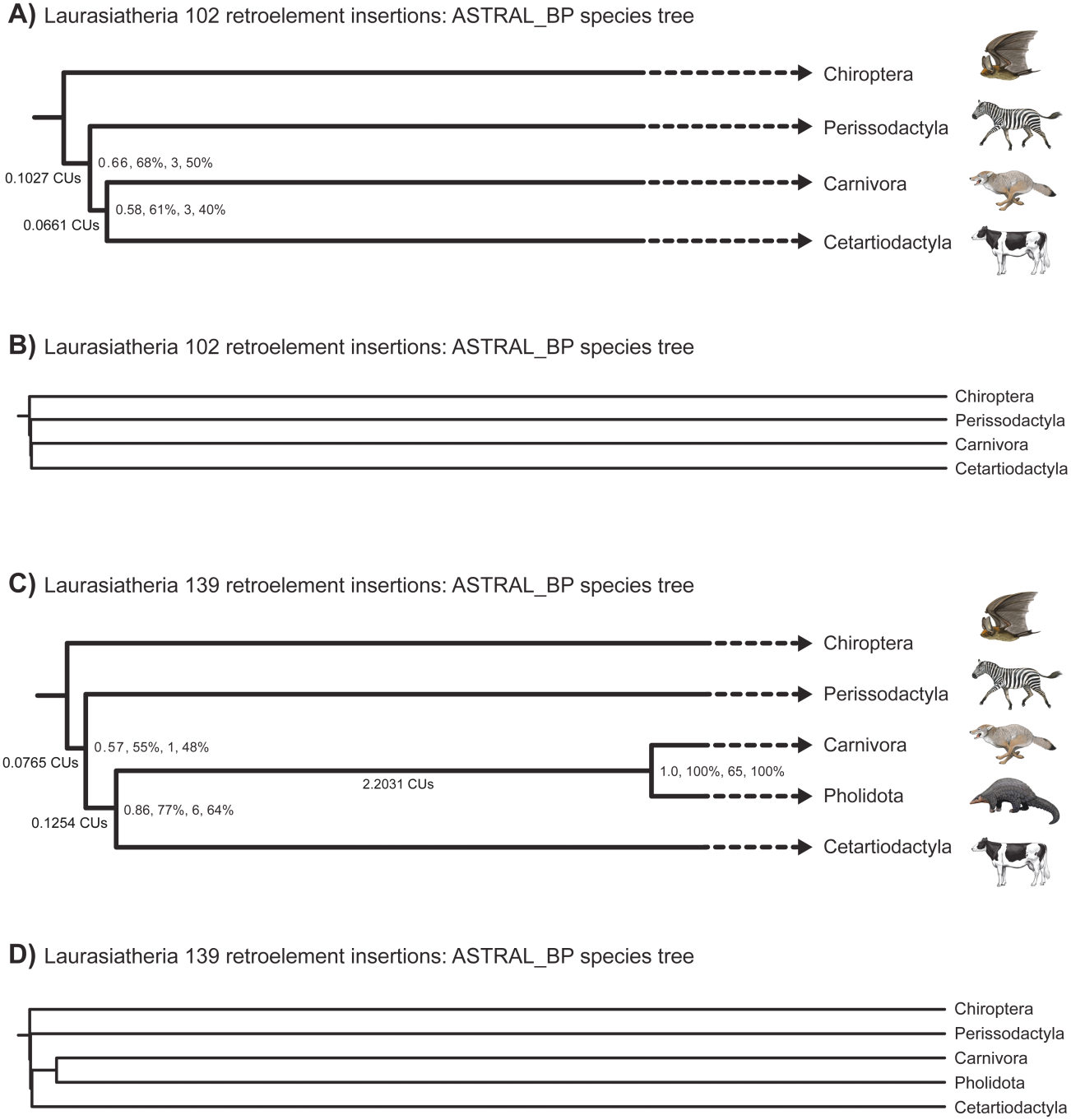

Figure 6. ASTRAL species trees for Laurasiatheria (**A**–**D**). The first 3 numbers at internal nodes correspond to local PP, ASTRAL bootstrap support percentage, and the minimum number of retroelement bipartitions that must be removed to collapse the clade in ASTRAL_BP analysis; the fourth number is the SDPquartets bootstrap percentage. Terminal branches are truncated in **A** and **C** so that the relative lengths of internal branches in coalescent units (CUs) can be seen. Species trees in **B** and **D** also show the entire internal branch lengths in CUs, demonstrating the extreme length of terminal branches relative to the very short internal branches that are barely visible. CU estimates for terminal branches are derived from molecular clock analyses (Meredith et al. 2011) because ASTRAL does not estimate terminal branch lengths. One million years from timetree estimates were converted to one CU (see Springer and Gatesy 2016 for rationale). Relationships in SDPquartets species trees are identical to those in the ASTRAL_BP species trees that are shown. The successive short branch lengths in CUs (0.1027 and 0.0661 for 5 taxa [**A** and **B**], 0.0765 and 0.1254 for 6 taxa [**C** and **D**]) in the species trees for Laurasiatheria are consistent with anomaly zone conditions (Degnan and Rosenberg 2006). The outgroup Eulipotyphla is not shown. Illustrations of mammals are by C. Buell.

to Carnivora (Figure 6C and D). However, posterior probabilities and bootstrap scores for interordinal relationships are low except for Carnivora + Pholidota (6 taxa). Carnivora + Pholidota collapses with the removal of 65 bipartitions (out of 139), but the other 2 internal branches collapse with the removal of just 1 to 6 bipartitions (out of 102 or 139) in ASTRAL_BP analyses (Figure 6A and C).

ASTRAL_BP branch lengths for the consecutive internal branches at the base of the Laurasiatheria trees are very short (0.1027 and 0.0661 for 5 taxa, 0.0765 and 0.1254 for 6 taxa) and are dwarfed

by the long terminal branch lengths of these trees (Figure 6B and D). The tiny internal branch lengths, along with the pectinate species tree for the 4 main lineages (Chiroptera, Perissodactyla, Cetartiodactyla, Carnivora + Pholidota), indicate that the virtual polytomy for Laurasiatheria may reside in the anomaly zone (Degnan and Rosenberg 2006, 2009) where the most likely gene tree topology differs from the species tree. Consistent with this interpretation, we simulated 10 000 genes trees from the 5-taxon ASTRAL_BP species tree, and the 3 most common gene tree topologies differ from the species tree. Specifically, all 3 of the symmetrical gene trees for the ingroup are better represented than the pectinate gene tree that agrees with the species tree. The symmetrical gene trees occur 1182 times ((Cetartiodactyla, Carnivora),(Perissodactyla, Chiroptera)), 1046 times (Cetartiodactyla, Perissodactyla), (Carnivora, Chiroptera)), and 991 times ((Cetartiodactyla, Chiroptera),(Carnivora, Perissodactyla)). By contrast, there are only 916 gene trees that match the species tree (Chiroptera,(Perissodact yla,(Carnivora, Cetartiodactyla))). An anomaly zone situation has also been suggested for palaeognath birds (Cloutier et al. 2019; Sackton et al. 2019), but in that case the consecutive short branches are more likely caused by conflicts from high reconstruction error for sequence-based gene trees, an interpretation that is corroborated by our analysis of retroelement insertion data from these birds (see below).

Doronina et al. (2017a) extended the KKSC test of Kuritzin et al. (2016) to a 4-lineage insertion likelihood test that allowed for different hybridization scenarios for Carnivora, Cetartiodactyla, Chiroptera, and Perissodactyla. This test did not include retroelement data for Eulipotyphla, which is the sister taxon to the remaining laurasiatherians. They applied this test to a data set that included 162 retroposon insertions and concluded that gene flow among lineages had occurred and that the most likely hybridization pathways were between 1) Perissodactyla and Chiroptera, 2) Perissodactyla and Carnivora, and 3) Perissodactyla and the common ancestor of Carnivora + Cetartiodactyla. We applied the Quartet-Asymmetry test to all 5 species quartets for the Laurasiatheria-102 data set by using an exact binomial test in R and found that there are no statistically significant differences between pairs of nonspecies-tree quartets (Table 1). We also examined these same 5 quartets for the Laurasiatheria-139 retroelement data set and again obtained nonsignificant results (Table 1). These results are consistent with ILS alone and do not require introgression (Table 1). The most extreme discrepancy in these comparisons is 20 versus 12 retroelement insertions for alternative nonspecies tree quartets, but the *P* value (0.215) for this comparison is not significant even without correcting for multiple comparisons. This result contrasts with Doronina et al.'s (2017a) conclusion that there is evidence for gene flow among basal laurasiatherian lineages based on their analysis of the 162 retroelement data set. However, there are important differences between the Quartet-Asymmetry test and Doronina et al.'s (2017a) 4-lineage insertion likelihood test. We applied the Quartet-Asymmetry test to all combinations of 4 taxa for 5 different orders (Carnivora, Cetartiodactyla, Chiroptera, Eulipotyphla, Perissodactyla), but as noted above Doronina et al. (2017a) did not consider Eulipotyphla and instead focused on different hybridization models for the remaining 4 orders. Also, the Quartet-Asymmetry test only indexes bipartitions that are informative for unrooted trees (i.e., 130 of 162 retroelement insertions for 5 taxa). By contrast, Doronina et al.'s (2017a) results are based on rooted trees and are influenced by all 162 retroelement insertions (see supplemental material S1 of Doronina et al. 2017a).

Balaenopteroidea Retroelements

Phylogenetic relationships among balaenopteroid species remain contentious based on previous phylogenetic analyses. Some studies support a sister-group relationship between Eschrichtiidae and

Table 1. The number of retroposons that support different splits for 5 different quartets of taxa that are associated with the Laurasiatheria polytomy[a]

Quartet of taxa	Split	102 Retroposon data set			139 Retroposon data set[b]		
		Obs. no. of quartets	Exp. no. of quartets under ILS	*P* value for Quartet-Asymmetry test[c]	Obs. no. of quartets	Exp. no. of quartets under ILS	*P* value for Quartet-Asymmetry test[c]
Eu, Pe, Ca, Ce	**Eu Pe | Ca Ce**	**22**		0.878	**25**		1.0
	Eu Ca | Pe Ce	22	21		22	21.5	
	Eu Ce | Pe Ca	20	21		21	21.5	
Eu, Pe, Ca, Ch	**Eu Ch | Ca Pe**	**25**		0.43	**25**		0.43
	Eu Ca | Pe Ch	23	20		23	20	
	Eu Pe | Ca Ch	17	20		17	20	
Eu, Pe, Ce, Ch	**Eu Ch | Pe Ce**	**24**		0.215	**24**		0.311
	Eu Ce | Pe Ch	20	16		21	17.5	
	Eu Pe | Ce Ch	12	16		14	17.5	
Eu, Ca, Ce, Ch	**Eu Ch | Ca Ce**	**28**		0.864	**31**		1.0
	Eu Ce | Ca Ch	18	17		19	18.5	
	Eu Ca | Ce Ch	16	17		18	18.5	
Pe, Ch, Ce, Ca	**Pe Ch | Ce Ca**	**25**		0.608	**38**		0.885
	Ch Ce | Pe Ca	15	17		25	24	
	Ch Ca | Pe Ce	19	17		23	24	

Obs., observed; Exp., expected; Ca, Carnivora; Ce, Cetartiodactyla; Ch, Chiroptera; Eu, Eulipotyphla; Pe, Perissodactyla.

[a]The species tree split for each quartet is shown in bold font.

[b]Compiled from Doronina et al.'s (2017a) supplemental table S1.

[c]*P* values are uncorrected and are based on the exact binomial test in R. We did not employ a correction for multiple tests because none of the *P* values were significant.

Balaenopteridae (e.g., Deméré et al. 2008; Steeman et al. 2009; Marx 2010; Gatesy et al. 2013), whereas Eschrichtiidae is resolved as nested inside of a paraphyletic Balaenopteridae in other studies (e.g., McGowen et al. 2009; Marx and Fordyce 2015). Figure 7A and B show the ASTRAL_BP species tree for balaenopteroids with internal branch lengths in CUs. Relationships in the SDPquartets topology are identical to those in the ASTRAL_BP tree. Bootstrap support percentages (ASTRAL_BP, SDPquartets), local PP values, and stability to removal of retroelement bipartitions are also shown in Figure 7A. The basal split in Balaenopteroidea is between minke whale and the other 5 balaenopteroids. Consistent with previous molecular studies (e.g., Rychel et al. 2004; Sasaki et al. 2005; Nikaido et al. 2006; Deméré et al. 2008; McGowen et al. 2009; Árnason et al. 2018), fin whale and humpback whale are sister taxa, and blue whale is closely related to sei whale. The gray whale is positioned as the sister taxon to the clade of fin whale + humpback whale. This coalescence-based retroelement topology matches a neighbor-joining distance analysis and a Bayesian inference tree for the same data (Lammers et al. 2019) as well as earlier studies based on molecular (McGowen et al. 2009; Árnason et al. 2018) and molecular + morphological data (Marx and Fordyce 2015). The branch that unites gray whale with the fin whale + humpback whale clade is very short (0.0182 CUs) on the ASTRAL_BP tree. Bootstrap support for this clade is 73% (SDPquartets) to 86% (ASTRAL_BP) and local PP is 0.88. The nested position of an eschrichtiid gray whale within Balaenopteridae renders this family paraphyletic (Figure 7A).

Overall, our species tree is robustly supported at most nodes and concordant with the ASTRAL tree that Árnason et al. (2018) reported for the same taxa based on gene trees for 34 192 genome fragments, each of which was 20 kb in length. Unlike retroelement gene trees (bipartitions), there are significant nonbiological contributors to gene tree heterogeneity when gene trees are inferred from DNA sequence alignments. These include long-branch misplacement, misaligned sequences, long tracts of missing data for one or more species, model misspecification, and paralogy problems. These issues can be partially mitigated by employing long segments of DNA (e.g., 20 kb segments of Árnason et al. 2018), but if these regions span one or more recombination breakpoints, multiple branching histories might be jumbled and violate the assumption of no intralocus recombination that underpins summary coalescent methods (Liu et al. 2009). Likewise, introgression of genetic material between lineages results in a patchwork of "native" and "foreign" DNA along chromosomes. If 20 kb segments include stretches of both native and foreign DNA, the assumption of a single underlying gene tree for each 20 kb segment would be violated. By contrast, the primary sources of conflict among retroelement insertions are biological and include ILS and/or introgression. This assumes that the presence/absence of retroelement insertions has been carefully scored in genomic screens (Doronina et al. 2019).

Árnason et al. (2018) inferred that extensive hybridization occurred in the evolutionary history of balaenopteroids based on network analysis of 34 192 gene trees with PhyloNET (Yu et al. 2014) and D_{FOIL}/D statistic (ABBA-BABA) tests on biallelic nucleotide sites (Durand et al. 2011; Pease and Hahn 2015). With these 2 approaches, they detected as many as 7 different gene flow signals (Figure 7C). Beyond these suggested historical pathways for introgression, there is also compelling genetic and phenotypic evidence for recent hybridization events between blue whales and fin whales (Bérubé and Aguilar 1998), as well as for a backcross between a female fin whale-blue whale hybrid and a male blue whale (Bérubé and Palsbøll 2018). In the presence of such gene flow, we do not expect the observed distribution of retroelements to be fully consistent with MSC expectations. Lammers et al. (2019) reported a dissonant pattern of CHR2 SINE insertions among balaenopteroids, but did not test whether the conflicting signal is the result of ILS alone or ILS plus introgression. Here, we reanalyzed the retroelement data set for Balaenopteroidea (Lammers et al. 2019) to test whether these data support the cases of introgression inferred by Árnason et al. (2018) using analyses of DNA sequences. We performed the Quartet-Asymmetry test (Figure 3) on 35 different quartets of species, and 19 of 35 tests were statistically significant at $P = 0.05$ following correction for multiple tests (Table 2).

The overall pattern of retroelement insertions is complex and includes multiple quartets of species with skewed support for alternative topologies relative to expectations based on ILS alone (Table 2, Figure 7D). Even with this complexity there are several themes that emerge from these comparisons. First, minke whale and blue whale are overrepresented in 3 different quartet tests, as are minke whale and sei whale in 3 tests. These results are consistent with Árnason et al.'s (2018) gene flow pathway I between the minke whale lineage and the common ancestral lineage of blue whale + sei whale (Figure 7C and D). Second, there is one significant quartet test that is consistent with gene flow between the gray whale lineage and the humpback whale lineage, which corresponds to Árnason et al.'s (2018) gene flow pathway III. Third, there are 4 asymmetry tests that are consistent with Árnason et al.'s (2018) gene flow pathway IV between the gray whale lineage and the blue whale lineage and/or the closely related gene flow pathway V between the gray whale and the common ancestral lineage of sei whale and blue whale. Fourth, there are 4 comparisons that are consistent with Árnason et al.'s (2018) gene flow pathway VII between the common ancestral lineage of humpback whale + fin whale and the blue whale lineage. Two of these 4 comparisons are also consistent with recently observed hybrids between fin and blue whales. The remaining comparisons with statistically significant P values provide evidence of gene flow pathways that are different from those suggested by Árnason et al. (2018). There is one significant quartet test for gene flow between the minke whale lineage and the humpback whale lineage. This is similar but not identical to Árnason et al.'s (2018) gene flow pathway II between the minke whale lineage and the common ancestral linage of humpback whale + fin whale. The next 2 overrepresented quartet splits are (right whale, fin whale|humpback whale, blue whale) and (right whale, fin whale|humpback whale, sei whale). These results are suggestive of introgression between the humpback whale lineage and the common ancestral lineage of blue whale + sei whale rather than Árnason et al.'s (2018) pathway VI between the common ancestral lineage of fin whale + humpback whale and the common ancestral lineage of blue whale + sei whale. Finally, there is an overrepresented split between (right whale, fin whale|minke whale, gray whale) that is consistent with hybridization between minke whale and gray whale (Table 2).

We note that the interaction of multiple gene flow pathways is expected to result in a complex pattern of retroelement insertions that does not necessarily translate into an overabundance of observed retroelement insertions for a particular alternative quartet. For example, hybridization between gray whale and humpback whale (path III of Árnason et al. 2018) will increase the proportion of retroelements that are shared between these 2 species in some quartets, but hybridization between gray whale and blue whale (path IV) and between gray whale and the common ancestral lineage of blue whale + sei whale (path V) are expected to have the opposite effect. These competing pathways of gene flow become even more complex

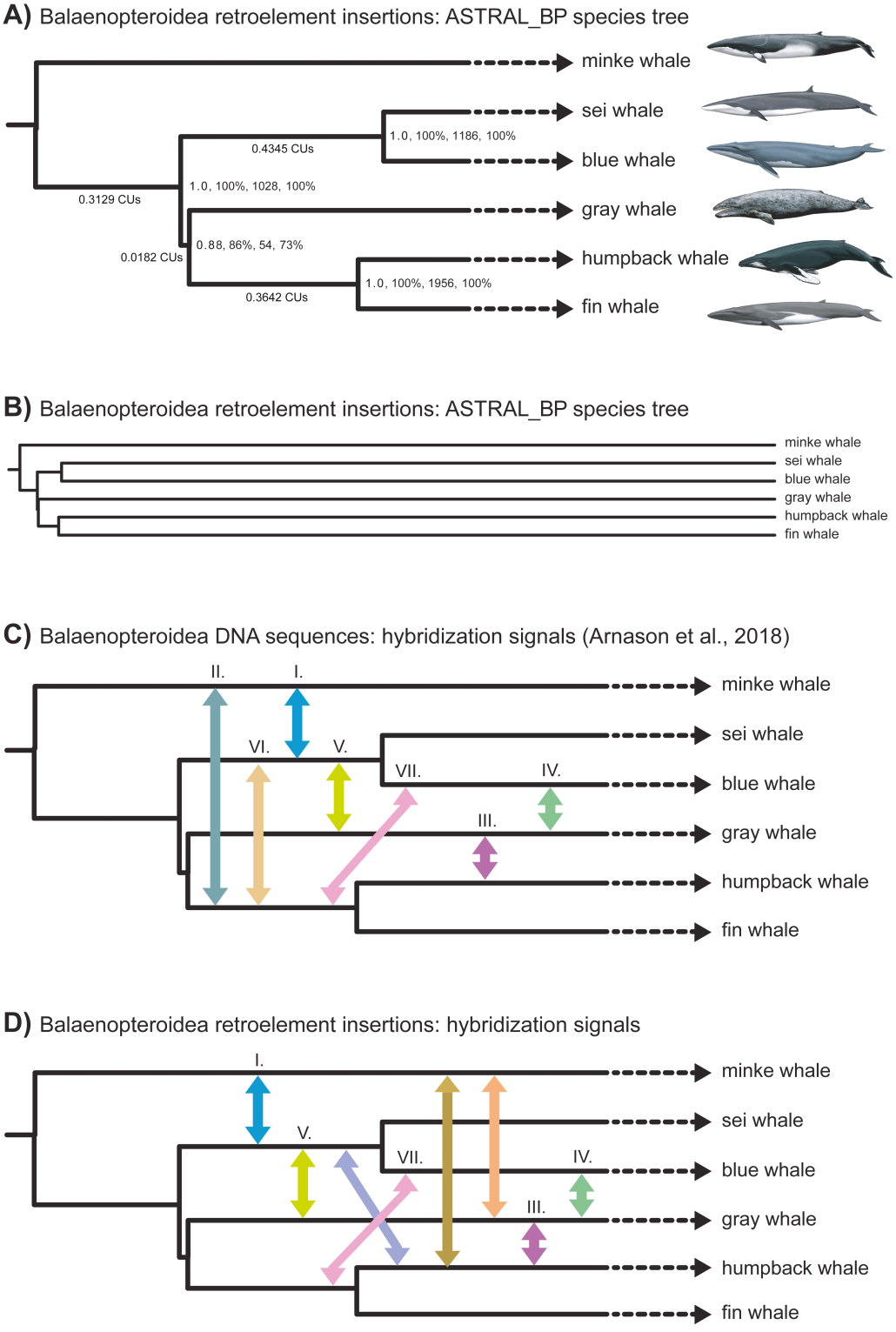

Figure 7. The ASTRAL_BP species tree for Balaenopteroidea based on 24 598 retroelement bipartitions (**A**–**D**). The first 3 numbers at internal nodes in **A** correspond to local PP, ASTRAL_BP bootstrap support percentage, and the minimum number of gene trees that must be removed to collapse the clade in ASTRAL_BP analysis; the fourth number is the SDPquartets bootstrap percentage. Terminal branches are truncated in **A**, **C**, and **D** so that relative lengths of internal branches in coalescent units (CUs) can be seen. The ASTRAL_BP species tree in **B** shows the entire branch lengths. CU estimates for terminal branches are derived from a molecular clock analysis (McGowen et al. 2009). One million years was converted to one CU (Springer and Gatesy 2016). Relationships in the SDPquartets species tree are identical to those in the ASTRAL_BP species tree that is shown. Árnason et al.'s (2018) 7 hypothesized pathways for introgression based on genomic sequences are shown in **C**. Possible gene flow pathways detected using the Quartet-Asymmetry test for retroelement insertions are shown in **D**. Note that 5 of Árnason et al.'s (2018) 7 hypothesized pathways are supported, whereas 2 are not. Also, 2 novel pathways are detected. Note that some pathways (e.g., VI) are necessarily historical and involve ancestral lineages rather than extant taxa. Illustrations of whales are by C. Buell.

if we consider past hybridization between the ancestor(s) of a living taxon and a completely extinct side-lineage of the clade (Maddison 1997; Rogers et al. 2019). For baleen whales, this is a nontrivial concern given that many extinct taxa have been described from this clade and species commonly share geographic ranges within ocean basins (Marx 2010; Marx and Fordyce 2015). Nevertheless, we infer an evolutionary history of hybridization in balaenopteroids based on significant retroelement asymmetry via several pathways that violate expectations based on ILS alone (Table 2; Figure 7D). If retroelements are coded properly without ascertainment bias, then comparisons of the observed and expected number of retroelements should not be complicated by gene tree reconstruction errors that can confound similar comparisons for gene trees that are based on sequence alignments (Song et al. 2012; Zhong et al. 2013; Jarvis et al. 2014; Liu et al. 2017).

Finally, we note that for a few quartets of taxa (e.g., blue whale, fin whale, gray whale, right whale) the number of retroelement insertions that agree with the species tree is less than the number of insertions that support one or both of the alternative trees (Table 2). This circumstance may result from an inaccurate species tree, sampling error, or introgression that overwhelms the correct species tree for a given quartet.

Palaeognathae Retroelements

Palaeognathae includes volant tinamous and the flightless ratites (ostrich, emu, rheas, kiwis, cassowaries). Recent analyses based on phylogenomic data sets have recovered conflicting phylogenetic hypotheses for this avian clade (Yonezawa et al. 2017; Cloutier et al. 2019; Sackton et al. 2019). All of these studies recovered a basal split between ostrich and other palaeognaths, but relationships among the non-ostrich palaeognaths differ in Yonezawa et al. (2017) versus the other 2 studies (Cloutier et al. 2019; Sackton et al. 2019). Yonezawa et al. (2017) suggested that rheas are the sister taxon to all other non-ostrich palaeognaths based on a supermatrix analysis of ~871 kb (also see ML concatenation tree of Prum et al. 2015), whereas Cloutier et al. (2019) and Sackton et al. (2019) recovered tinamous as the extant sister group to all other extant non-ostrich palaeognaths based on summary coalescent analyses with MP-EST and ASTRAL on 20850 loci (Figure 8A and B). Yonezawa et al.'s (2017) topology was corroborated by supermatrix analyses of the 20850 loci compiled by Sackton et al. (2019) that also placed rheas as sister to all other non-ostrich palaeognaths. Sackton et al. (2019) and Cloutier et al. (2019) suggested that very short branches on their MP-EST species tree (Figure 8A) provide evidence for an "empirical anomaly zone" in palaeognaths that misled concatenation analyses. Specifically, the consecutive and very short branches of 0.3657, 0.0632, and 0.0662 CUs on their MP-EST tree are the primary evidence for asserting that the palaeognath tree resides in the anomaly zone (Cloutier et al. 2019; Sackton et al. 2019). The 2 shortest branches are even shorter (0.0194, 0.0532) on Cloutier et al.'s (2019) ASTRAL species tree (Figure 8B). Consistent with their anomaly zone inference, the most common gene tree in their analysis differs from the inferred species tree as predicted by theoretical work (Degnan and Rosenberg 2006, 2009). Sackton et al. (2019) also reported that retroelement insertions from Cloutier et al. (2019) provide independent support for their preferred phylogenetic hypothesis, although the retroelements were not analyzed with ILS-aware methods in these studies.

We reanalyzed the retroelement data set (4301 insertion characters, 13 taxa) with ASTRAL_BP and SDPquartets and the resulting species tree is robustly supported (Figure 8C and D). All relationships agree with the MP-EST and ASTRAL species trees based on DNA sequence alignments (Figure 8A and B; Cloutier et al. 2019; Sackton et al. 2019), but a fundamental difference is that internal branch lengths (in CUs) are much longer on the ASTRAL_BP species tree based on retroelements (Figure 8C and D). On average, internal branch lengths on the retroelement species tree are ~4.8× longer than the corresponding internal branches on the MP-EST species tree, including the 3 branches that make or break the anomaly zone (Figure 8C). First, the common ancestral branch for all palaeognaths except ostrich is 2.539 CUs on the retroelement tree but only 0.3657 CUs on the MP-EST tree. Second, the most striking discrepancy is for the internal branch leading to the clade of rheas, kiwis, emu, and cassowary where the ASTRAL_BP branch length (0.8938 CUs) is ~14.1× longer than the same branch (0.0632 CUs) on the MP-EST tree constructed from DNA sequence-based gene trees. Finally, the internal branch leading to kiwis, emu, and cassowary is 0.2528 CUs on the ASTRAL_BP tree but only 0.0662 CUs on the MP-EST tree.

We used the ASTRAL_BP species tree with its estimates of branch lengths in CUs (Figure 8C and D) to simulate 10 000 gene trees with DendroPy v3.12.0 (Sukumaran and Holder 2010). The most common gene tree topology is congruent with the ASTRAL_BP species tree based on retroelements and accounts for 14.9% of the simulated trees. The next most common gene tree was a distant 7.28% of the total. These results contrast strikingly with the distribution of gene tree topologies based on analyses of DNA sequence data, for which the most common gene trees disagree with the species tree (Sackton et al. 2019), and only ~240 of the 20 850 gene trees (1.15%) match the MP-EST species tree (Cloutier et al. 2019; Sackton et al. 2019).

In addition to ILS, topological gene tree heterogeneity may result from gene tree reconstruction error (e.g., due to long branch misplacement, misalignment of nonhomologous sequences, model misspecification) and arbitrary resolution of polytomies. The latter problem is common in phylogenomic studies where RAxML and/or PhyML are used to reconstruct gene trees from sequence data (Gatesy and Springer 2014; Simmons and Norton 2014; Simmons and Randle 2014). Given that Sackton et al. (2019) and Cloutier et al. (2019) used RAxML to reconstruct gene trees, we applied the Shimodaira-Hasegawa-like approximate likelihood-ratio test (SH-like aLRT; Anisimova and Gascuel 2006; Guindon et al. 2010) to their posted 20 850 MAFFT-alignment gene trees to determine the fraction of clades that are the result of arbitary resolution in their RAxML-derived gene trees. RAxML only ever presents to the user a single fully resolved optimal gene tree irrespective of whether or not the clades are unambiguously supported by the data (e.g., Simmons and Norton 2014; Simmons and Randle 2014). The SH-like aLRT, which is implemented in RAxML, tests if resolution of each internal branch provides a significant increase in likelihood relative to either collapsing that branch or the 2 alternative nearest-neighbor-interchange resolutions of the internode. Clades with ~zero length branches as well as those that are absent in the strict consensus of slightly suboptimal trees generally are assigned 0% SH-like aLRT support (Simmons and Kessenich 2019). Of the 224 257 internal branches in the 20 850 gene trees, 55 269 (24.6%) received 0% SH-like aLRT support, and hence are unsupported and arbitrarily resolved. Thus, one would expect that many of these internal branches are not accurate reconstructions.

As noted above, the consecutive short branches of 0.3657, 0.0632, and 0.0662 CUs on the palaeognath MP-EST tree (Figure 8A) and similarly short branch lengths for the ASTRAL

Table 2. Mysticete quartets with statistically significant asymmetry for introgression[a]

Quartet of taxa	Split	Obs. no. of quartets	Exp. no. of quartets under ILS	χ^2	*P* value uncorrected/ *P* value corrected[b]	Introgression pathway[c]
RW, MW, GW, SW	**RW MW|GW SW**	**3210**		24.54	7.26E-07/ 1.52E-05	I (MW <–> SW + BW)
	RW GW|MW SW	1749	1608.5			
	RW SW|MW GW	1468	1608.5			
RW, MW, GW, BW	**RW MW|GW BW**	**3684**		51.46	7.31E-13/ 1.10E-10	I (MW <–> SW + BW)
	RW GW|MW BW	1813	1609.5			
	RW BW|MW GW	1406	1609.5			
RW, MW, FW, SW	**RW MW|FW SW**	**3055**		66.72	3.33E-16/ 1.10E-10	I (MW <–> SW + BW)
	RW FW|MW SW	1853	1620.5			
	RW SW|MW FW	1388	1620.5			
RW, MW, FW, BW	**RW MW|FW BW**	**3480**		104.61	0.0E-10/ 0.0E-10	I (MW <–> SW + BW)
	RW FW|MW BW	1965	1669.5			
	RW BW|MW FW	1374	1669.5			
RW, MW, HW, SW	**RW MW|HW SW**	**3168**		24.47	7.56E-07/ 1.52E-05	I (MW <–> SW + BW)
	RW HW|MW SW	1683	1545.5			
	RW SW|MW HW	1408	1545.5			
RW, MW, HW, BW	**RW MW|HW BW**	**3578**		52.16	5.12E-13E/ 0.0E-10	I (MW <–> SW + BW)
	RW HW|MW BW	1742	1541.5			
	RW BW|MW HW	1341	1541.5			
RW, GW, FW, HW	**RW GW|FW HW**	**3318**		27.52	1.55E-07/ 3.41E-06	III (GW <–> HW)
	RW FW|GW HW	1695	1549			
	RW GW|FW HW	1403	1549			
RW, BW, GW, FW	**RW BW|GW FW**	**1779**		29.09	6.89E-08/ 1.58E-06	IV and V (GW <–> BW)
	RW GW|FW BW	2000	2178			
	RW FW|GW BW	2356	2178			
RW, GW, SW, BW	**RW GW|SW BW**	**3948**		97.85	1E-10/ 0.0E-10	IV and V (GW <–> BW)
	RW SW|GW BW	1736	1468			
	RW BW|GW SW	1200	1468			
MW, GW, SW, BW	**MW GW|SW BW**	**3726**		52.86	3.58E-13/ 0.0E-10	IV and V (GW <–> BW)
	MW SW|GW BW	1795	1590			
	MW BW|GW SW	1385	1590			
RW, GW, FW, SW	**RW SW|GW FW**	**2074**		16.89	3.96E-05	V (GW <-> SW)
	RW FW|GW SW	2115	1985.5			
	RW GW||FW SW	1856	1985.5			
MW, FW, SW, BW	**MW FW|SW BW**	**3754**		32.78	1.03E-08/ 2.68E-07	VII (BW <–> FW + HW); also observed BW <–> FW in nature
	MW SW|FW BW	1651	1494.5			
	MW BW|FW SW	1338	1494.5			
MW, HW, SW, BW	**MW HW|SW BW**	**3666**		40.57	1.90E-10/ 5.1E-09	VII (BW <–> FW + HW)
	MW SW|HW BW	1694	1518.5			
	MW BW|HW SW	1343	1518.5			
RW, HW, SW, BW	**RW HW|SW BW**	**3845**		83.68	1E-10/ 1.10E-10	VII (BW <–> FW + HW)
	RW SW|HW BW	1598	1359.5			
	RW BW|HW SW	1121	1359.5			
RW, FW, SW, BW	**RW FW|SW BW**	**4108**		72.97	1E-10/ 1.10E-10	VII (BW <–> FW + HW); also observed BW <–> FW in nature
	RW SW|FW BW	1540	1320.5			
	RW BW|FW SW	1101	1320.5			
RW, MW, FW, HW	**RW MW|FW HW**	**4824**		16.13	5.91E-05/ 1.06E-03	MW <-> HW
	RW FW|MW HW	1214	1119			
	RW HW|MW FW	1024	1119			
RW, BW, FW, HW	**RW BW|FW HW**	**3131**		32.25	1.36E-08/ 3.40E-07	HW <–> BW + SW
	RW FW|HW BW	1758	1597.5			
	RW HW|FW BW	1437	1597.5			
RW, SW, FW, HW	**RW SW|FW HW**	**3349**		29.50	5.60E-08/ 1.34E-06	HW <–> BW + SW
	RW FW|HW SW	1499	1357.5			
	RW HW|FW SW	1216	1357.5			
RW, MW, GW, FW	**RW MW|GW FW**	**3388**		10.61	1.12E-03/ 1.90E-02	MW <-> GW
	RW GW|MW FW	1503	1595			
	RW FW|MW GW	1687	1595			

Obs., observed; Exp., expected; BW, blue whale; FW, fin whale; GW, gray whale; HW, humpback whale; MW, minke whale; RW, North Atlantic right whale; SW, sei whale.

[a]The species tree split for each quartet is shown in bold font. The Quartet-Asymmetry test was performed with a χ^2 test.

[b]Corrected for multiple comparisons using a Holm-Bonferroni test with Gaetano's (2018) Excel calculator (1.3).

[c]Roman numerals correspond to introgression pathways of Árnason et al. (2018).

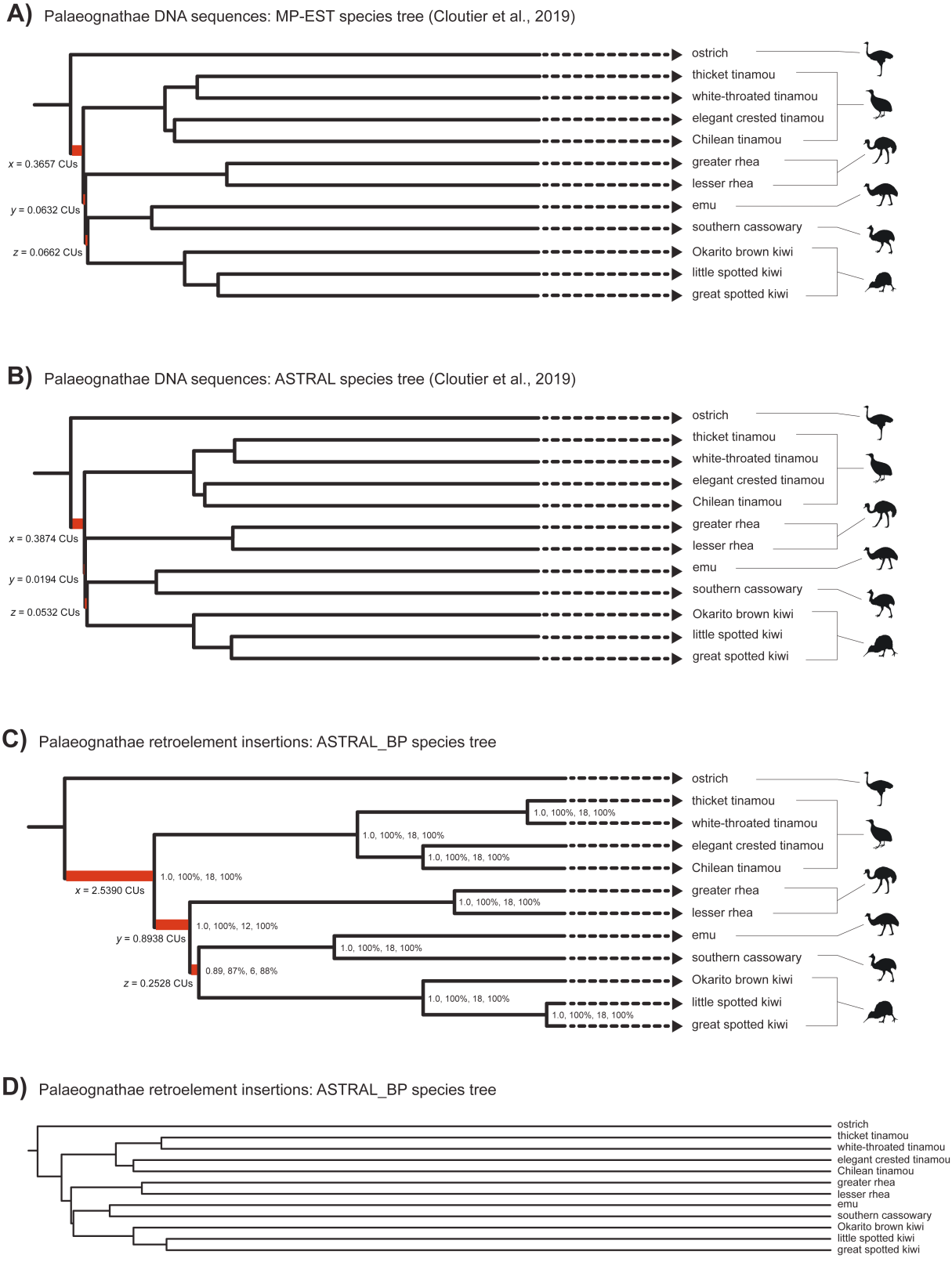

Figure 8. Species tree estimates for Palaeognathae based on summary coalescence methods: (**A**) MP-EST species tree derived from analysis of 20 850 sequence-based gene trees (Cloutier et al. 2019; Sackton et al. 2019), (**B**) ASTRAL species tree derived from analysis of 20 850 sequence-based gene trees (Cloutier et al. 2019), and (**C** and **D**) ASTRAL_BP species tree derived from analysis of 4301 retroelement insertions characterized by Cloutier et al. (2019). Internal branch lengths in coalescent units (CUs) are to the same scale in **A**, **B**, and **C**, and terminal branch lengths are truncated. The ASTRAL_BP retroelement tree in **C** is at a lower scale in **D** to show the long terminal branches relative to the shorter internal branches. CU estimates for terminal branches are derived from a molecular clock

analysis of the same sequence data (Figure 8B) are the primary evidence for asserting that the palaeognath species tree resides in an "empirical anomaly zone" (Cloutier et al. 2019; Sackton et al. 2019). If we view the early palaeognath radiation as a 5-taxon problem (ostrich, tinamous, rheas, emu + cassowaries, and kiwis), then the 3 internal branches that define relationships among these lineages may each have a maximum value of 0.1934 CUs if the rooted species tree is in the anomaly zone and if the 3 branches are coequal in length (Rosenberg and Tao 2008; Degnan and Rosenberg 2009). One or two of these branches may be longer in the anomaly zone, but only if the other branches compensate by being shorter (see length limits for branches *x*, *y*, and *z* in figure 4 of Rosenberg 2013). In the case of a 4-taxon problem (tinamous, rheas, emu + cassowaries, and kiwis), the 2 internal branches may each have a maximum value of 0.156 CUs in order for the rooted species tree to be in the anomaly zone if the branches are coequal in length (Degnan and Rosenberg 2006). If the basal branch length (*x*) is >0.2655 then the anomaly zone is not applicable for the 4-taxon case (Degnan and Rosenberg 2006). Sackton et al.'s (2019) MP-EST tree has 3 consecutive branches (*x*, *y*, *z*) that are consistent with an anomaly zone situation for 5 taxa (Rosenberg 2013), including 2 branches that are <0.1934 CUs (Figure 8A). Similarly, Sackton et al.'s (2019) MP-EST tree is consistent with an anomaly zone situation for 4 taxa, and Cloutier et al.'s (2019) ASTRAL species tree for sequence-based gene trees also has branch lengths that imply an anomaly zone for both the 4 and 5 taxon cases (Figure 8B). However, there are no internal branches on our ASTRAL_BP retroelement tree that are below 0.1934 CUs (Figure 8C) for the 5-taxon case or below 0.156 CUs for the 4-taxon case. For the Palaeognathae retroelement data set, we used gene-wise bootstrap resampling (Simmons et al. 2019) with ASTRAL_BP to pseudoreplicate 100 species trees with branch lengths in CUs. In every case, the branch lengths (*x*, *y*, *z*) on these ASTRAL_BP retroelement species trees are not short enough to warrant an anomaly zone interpretation in either the 4- or 5-taxon case.

The internal branch lengths in the sequence-based species trees (Figure 8A and B) and the retroelement-based species tree (Figure 8C and D) tell 2 very different stories about the early diversification of palaeognaths. For example, 18 retroelement insertions show uniform support, with no conflicts, for the clade that includes all palaeognaths except the ostrich (Cloutier et al. 2019), suggesting limited ILS. By contrast, sequence-based gene trees show extensive conflict at this node (69% for conserved nonexonic elements, 39% for UCEs, 35% for introns). We contend that the much longer internal branch lengths on the retroelement species tree for this clade and others are more accurate than the much shorter branch lengths on Sackton et al.'s (2019) MP-EST species trees. This is because gene tree reconstruction error is negligible for retroelements (Doronina et al. 2019), but not for sequence-based gene trees at deep divergences (Huang and Knowles 2009; Huang et al. 2010; Springer and Gatesy 2014, 2016, 2018a, 2018b; Bayzid et al. 2015; Mirarab and Warnow 2015; Simmons and Gatesy 2015; Sayyari and Mirarab 2016; Gatesy et al. 2017; Sayyari et al. 2017; Scornavacca and Galtier 2017; Molloy and Warnow 2018). Cloutier et al. (2019, p. 16) noted that an "important and related question is whether we can confidently detect an empirical anomaly zone given that the same short internal branches expected to produce anomalous gene trees also increase the likelihood of gene tree estimation error due to the short time interval for informative substitutions to accumulate in individual loci of finite length (Huang and Knowles, 2009)." The retroelement data collected by these authors provide an answer to this question when converted to bipartitions and analyzed with ASTRAL. Specifically, the branch lengths on the ASTRAL-BP species tree are well outside of the anomaly zone (Figure 8C and D). Furthermore, arbitrary resolution of more than 24% of the nodes in Cloutier et al.'s (2019) gene trees reiterates these authors' worries about extensive gene tree conflicts due to lack of informative variation at short internodes.

Finally, we used an exact binomial test to implement the Quartet-Asymmetry test for 5 quartets from the Palaeognathae data set. These quartets sample one representative from each of the 5 major lineages (ostrich, tinamous, rheas, emu/cassowary, kiwis) and index the early radiation of this clade. However, there is no evidence for introgression based on these analyses (Table 3). Instead, the number of retroelements that support each of the 2 nonspecies-tree quartets is in agreement with expectations under ILS only (Table 3). Moreover, the number of retroelements that support each species tree quartet always exceeds the number of retroelements that conflict with the species tree quartet. By contrast, retroelement support for the 3 competing hypotheses (species tree quartet and conflicting quartets) is more evenly split for the Laurasiatheria data set (Table 1) than for Palaeognathae. Specifically, the number of retroelements that support each species tree quartet for Laurasiatheria is always much less than the sum of retroelements that support the 2 conflicting quartets. These results suggest that ILS is more problematic for resolving the Laurasiatheria polytomy than for the early radiation of Palaeognathae.

Gene Tree Reconstruction Error, ILS, and the Anomaly Zone

Previous studies repeatedly have shown that branch lengths (in CUs) on coalescence-based species trees are stunted because of gene tree reconstruction error, which mimics conflict due to ILS (Gatesy and Springer 2014; Mirarab et al. 2014a, 2014b; Springer and Gatesy 2014, 2016, 2018a, 2018b; Bayzid et al. 2015; Roch and Warnow

analysis (Jarvis et al. 2014) because ASTRAL does not estimate terminal branch lengths. One million years from the timetree estimate were converted to one CU (Springer and Gatesy 2016). Note the disparity of internal branch lengths between the retroelement-based species tree (**C**) and the 2 species trees based on DNA sequence gene trees (**A** and **B**) at the base of Palaeognathae. Internal branches for the ASTRAL_BP retroelement tree are much longer. The 3 internal branches that comprise the "empirical anomaly zone" of Sackton et al. (2019) are colored red and labeled x, y, and z as in Rosenberg (2013). Support scores for the ASTRAL_BP retroelement tree (**C**) are shown at internal nodes (Bayesian local PP, ASTRAL bootstrap support percentage, minimum number of retroelement bipartitions that must be removed to collapse the clade), and also SDPquartets bootstrap percentages. All clades in the MP-EST tree (**A**) received 100% support for the multilocus bootstrap, and all clades in the ASTRAL tree (**B**) had Bayesian local PP of 1.0 (Cloutier et al. 2019; Sackton et al. 2019). All species trees are rooted with chicken (*Gallus*) outgroup (not shown), and 2 taxa (North Island brown kiwi, little bush moa) that were not sampled in the retroelements data set were pruned from the DNA-sequence-based species trees (**A** and **B**). Internal branch lengths for the MP-EST species tree are from the "TENT_mafft_MP-EST_run1.tre"file of Sackton et al. (2019); branch lengths are similar for other MP-EST species trees posted by these authors; branch lengths for the ASTRAL species tree are from the "TENT_astral_species_tree.tre" file of Cloutier et al. (2019). Silhouettes of tinamou, kiwi, and cassowary are freely available from PhylPic (http://phylopic.org/; Public Domain Mark 1.0 license). Silhouettes for ostrich (credit to Matt Martyniuk [vectorized by T. Michael Keesey]; https://creativecommons.org/licenses/by-sa/3.0/) and rhea plus emu (Darren Naish [vectorized by T. Michael Keesey]; https://creativecommons.org/licenses/by/3.0/) also were downloaded from PhyloPic.

Table 3. The number of retroposons that support different splits for 5 different quartets of taxa that are associated with the early radiation of Palaeognathae[a]

Quartet of taxa	Split	Obs. no. of quartets	Exp. no. of quartets under ILS	*P* value for Quartet-Asymmetry test[b]
CT, GR, GK, E	**CT GR |GK E**	**15**		1.0
	CT GK|GR E	7	6.5	
	CT E|GK GR	6	6.5	
O, CT, E, GR	**O CT|E GR**	**11**		0.625
	O E|CT GR	3	2	
	O GR|CT E	1	2	
O, CT, GK, GR	**O CT|GK GR**	**10**		0.625
	O GK|CT GR	3	2	
	O GR|CT GK	1	2	
O, CT, E, GK	**O CT|E GK**	**17**		1.0
	O E|CT GK	1	1	
	O GK|CT E	1	1	
O, GR, E, GK	**O GR|E GK**	**12**		1.0
	O E|GK GR	5	5.5	
	O GK|E GR	6	5.5	

Obs., observed; Exp., expected; CT, Chilean tinamou; E, emu; GK, great spotted kiwi; GR, greater rhea; O, ostrich.

[a]The species tree split for each quartet is shown in bold font.

[b]*P* values are uncorrected and are based on the exact binomial test in R. We did not employ a correction for multiple tests because none of the *P* values were significant.

2015). Retroelement insertions and sequence-based gene trees for the phylogenetic placement of tarsiers within primates provide an excellent example of the gene-tree reconstruction error problem (Supplementary Figure S1; Gatesy and Springer 2014; Gatesy et al. 2017; Springer and Gatesy 2018b). More generally, we argue that much of the gene tree heterogeneity in sequence-based analyses at deep divergences is unrelated to ILS and instead results from long branch misplacement, model misspecification, lack of phylogenetic signal, arbitrary resolution (see above), missing data, homology problems, and poor tree searches (Gatesy and Springer 2013, 2014; Patel et al. 2013; Springer and Gatesy 2014, 2016, 2017, 2018a, 2018b, 2018c; Gatesy et al. 2017, 2019). Such gene tree reconstruction errors artificially inflate conflicts and are known to result in bonsai species trees (MP-EST and ASTRAL) with highly stunted internal branches (Gatesy and Springer 2014; Mirarab et al. 2014a, 2014b; Springer and Gatesy 2014, 2016, 2018b; Bayzid et al. 2015; Roch and Warnow 2015). In the case of palaeognaths, the much longer internal branches on our retroelement species tree therefore call into question the existence of an "empirical anomaly zone" for Palaeognathae (Figure 8).

Cloutier et al. (2019, p. 13) used simulations of gene trees from their MP-EST species tree with tiny internal branches (Figure 8A) to "assess what proportion of total gene tree heterogeneity is likely attributable to coalescent processes rather than to gene tree estimation error" and found that 70–90% of the gene tree conflict is compatible with ILS. However, previous work has shown that this simulation procedure is flawed because of gene tree reconstruction error that stunts branches on sequence-based MP-EST species trees and is therefore a poor phylogenetic model for subsequent simulation of gene trees (Springer and Gatesy 2014, 2016, 2018a, 2018b; Gatesy et al. 2017). Indeed, we have shown that almost 25% of nodes in the sequence-based gene trees of Cloutier et al. (2019) are arbitrarily resolved. By contrast, retroelement insertions can be more reliably reconstructed due to very low levels of homoplasy at single genomic sites (Doronina et al. 2019). In accordance with this expectation, the palaeognath species tree based on retroelements has ~4.8× longer internal branch lengths than the species tree that was reconstructed from sequence-based gene trees (Cloutier et al. 2019; Sackton et al. 2019). Furthermore, branch lengths on the retroelement species tree for palaeognaths are inconsistent with the "empirical anomaly zone" hypothesis (Figure 8C).

Applications of ILS-Aware Methods to Other Types of Bipartition Data

ASTRAL_BP and SDPquartets were developed to infer species trees with retroelements. However, these methods are generally applicable to other bipartition characters if they satisfy or approximate the assumptions of the multispecies coalescent including no intralocus recombination, free recombination among loci, no gene tree reconstruction error (i.e., no homoplasy or homology errors), and neutral evolution. Bipartition characters that are good candidates to satisfy at least some of these assumptions include several classes of rare genomic changes such as large insertions and deletions (indels), nuclear DNA sequences of mitochondrial origin (NUMTs), gains or losses of introns, and chromosomal rearrangements (e.g., inversions, translocations) (Rokas and Holland 2000; Han et al. 2011; Liang et al. 2018). The Quartet-Asymmetry test may also be applied to test for introgression with these bipartition characters. For example, Schull et al. (2019) recently characterized large (>75 bp) indels that support alternative relationships among the paenungulate orders Sirenia (manatees and dugongs), Proboscidea (elephants), and Hyracoidea (hyraxes). Four hundred twenty-two long indels support Sirenia + Proboscidea, 242 support Proboscidea + Hyracoidea, and just 54 support Sirenia + Hyracoidea. If Sirenia + Proboscidea, the dominant indel pattern, represents the species tree, then there is strong evidence for introgression between the hyracoid and proboscidean lineages according to the Quartet-Asymmetry test ($P < 2.2e\text{-}16$ based on exact binomial test).

Conclusions

Retroelement insertions provide an important alternative to DNA sequence alignments for inferring species trees. This is because ILS-aware analyses of retroelements avoid many of the well-documented

challenges that can plague the practical application of summary (gene tree) and single-site coalescent methods to real DNA sequences. First, retroelement insertions are singular events that are subject to interlocus recombination and ILS, but the presence/absence of a retroelement is not impacted by intralocus recombination. Second, gene tree reconstruction error is minimized because retroelement insertions have very low rates of homoplasy. Importantly, retroelements retain signal at deep divergences in the Tree of Life because of these low levels of homoplasy. Finally, many or perhaps most retroelement insertions occur in genomic safe havens where they are tolerated by natural selection and may be effectively neutral.

We analyzed 5 retroelement data sets (Placentalia, Laurasiatheria-102, Laurasiatheria-139, Balaenopteroidea, Palaeognathae) with ASTRAL_BP and SDPquartets (Figure 2) to infer species trees that are in general agreement with previous analyses (Nishihara et al. 2009; Doronina et al. 2017a; Cloutier et al. 2019; Lammers et al. 2019; Sackton et al. 2019). Our coalescence analyses of Laurasiatheria retroelements further identified a possible case of the anomaly zone based on consecutive short branch lengths of 0.1027 and 0.0661 CUs (5 taxa) or 0.0765 and 0.1254 CUs (6 taxa) (Degnan and Rosenberg 2006, 2009) (Figure 6) for lineage splits that likely occurred in the Upper Cretaceous (Meredith et al. 2011). By contrast, an ILS-aware analysis of Palaeognathae retroelements recovered a species tree with estimated branch lengths that are outside of the anomaly zone (Figure 8C and D). This analysis of Palaeognathae retroelements disagrees with previous interpretations of DNA sequence-based species trees for this clade that are characterized by stunted internal branch lengths (Figure 8A and B; Cloutier et al. 2019; Sackton et al. 2019).

The analysis of retroelements with ILS-aware methods offers hope for resolving rapid radiations that are deep in evolutionary history. We further demonstrate the utility of retroelement data for discerning ancient hybridization events using a simple but general Quartet-Asymmetry test (Figure 3). As for the application of ABBA-BABA tests (D statistic) to DNA sequence data (Green et al. 2010), significant results for this test suggest that ILS alone is insufficient to explain highly skewed distributions of shared genetic changes for particular species quartets. Introgression is a plausible explanation for this pattern because other sources of gene tree heterogeneity such as gene tree reconstruction error and intralocus recombination are thought to be inconsequential when retroelement insertions are conservatively coded and without ascertainment bias (Doronina et al. 2019). More specifically, variables such as lineage-specific rate variation and heterogeneous base compositional shifts over deep time can drive asymmetry in support for alternative quartets based on DNA sequence alignments (Pease et al. 2018), but retroelement insertions should be immune to these problems.

In the case of Balaenopteroidea, comparisons between observed and expected distributions suggest that ILS alone cannot account for the observed distribution of retroelements in the genomes of these whales. By contrast, retroelement insertions for Laurasiatheria, Placentalia, and Palaeognathae are consistent with ILS expectations. We suggest that our general test for asymmetry in retroelement patterns, which allows for all possible outcomes of ILS (e.g., Figures 1 and 4), offers a valuable framework for the analysis of ancient hybridization events across the Tree of Life in lineages where retroelements were active. The development of novel phylogenetic methods that simultaneously consider both ILS and introgression (Yu et al. 2014; Solís-Lemus et al. 2016) should be a priority in future systematic studies that utilize retroelement insertions. Methods that only allow for ILS may recover an incorrect species tree in the context of introgression, even when homoplasy is only a minor issue for retroelement insertions. If there is evidence for introgression, then retroelements may be especially useful for teasing apart regions of the genome with different histories. Specifically, retroelements in one region of the genome may track initial speciation (cladogenesis) whereas retroelements in a different region of the genome may provide evidence for more recent gene flow (Li et al. 2019). In this context, the distribution of retroelements in different regions of the genome should enable meaningful comparisons with previous hypotheses for introgression based on sequence-based analyses (Li et al. 2016, 2019; Árnason et al. 2018).

Supplementary Material

Supplementary data are available at *Journal of Heredity* online.

Funding

This work was supported by the National Science Foundation (DEB-1457735 to J.G. and M.S.S.; IOS-1829176 to D.B.S.).

Acknowledgments

C. Buell provided images of mammals. Several anonymous reviewers provided helpful comments on this article.

Data Availability

Retroelement data matrices, optimal gene trees (with branch lengths in CUs), bootstrap trees, and other supplemental files associated with this study are posted at: https://figshare.com/s/9a2180de2ab4a6ce2162.

References

Abo H, Seigal A, Sturmfels B. 2017. Algebraic and geometric methods in discrete mathematics. In: Harrington A, Omar M, Wright M, editors. Contemporary mathematics. Vol. 685. Providence (RI): American Mathematical Society. p. 1–25.

Allman ES, Degnan JH, Rhodes JA. 2011. Identifying the rooted species tree from the distribution of unrooted gene trees under the coalescent. *J Math Biol*. 62:833–862.

Ané C. 2010. Reconstructing concordance trees and testing the coalescent model from genome-wide data sets. In: Knowles LL, Kubatko LS, editors. Estimating species trees: practical and theoretical aspects. Hoboken (NJ): Wiley-Blackwell. p. 35–52.

Anisimova M, Gascuel O. 2006. Approximate likelihood-ratio test for branches: a fast, accurate, and powerful alternative. *Syst Biol*. 55:539–552.

Árnason Ú, Lammers F, Kumar V, Nilsson MA, Janke A. 2018. Whole-genome sequencing of the blue whale and other rorquals finds signatures for introgressive gene flow. *Sci Adv*. 4:eaap9873.

Avise JC, Robinson TJ. 2008. Hemiplasy: a new term in the lexicon of phylogenetics. *Syst Biol*. 57:503–507.

Bannert N, Kurth R. 2004. Retroelements and the human genome: new perspectives on an old relation. *Proc Natl Acad Sci U S A*. 101 (Suppl 2):14572–14579.

Bayzid MS, Mirarab S, Boussau B, Warnow T. 2015. Weighted statistical binning: enabling statistically consistent genome-scale phylogenetic analyses. *PLoS One*. 10:e0129183.

Bérubé M, Aguilar A. 1998. A new hybrid between a blue whale, *Balaenoptera musculus*, and a fin whale, *B. physalus*: frequency and implications of hybridization. *Mar Mamm Sci*. 14:82–98.

Bérubé M, Palsbøll PJ. 2018. Hybridism. In: *Encyclopedia of marine mammals*. London (UK): Academic Press. p. 496–501.

Blom MPK, Bragg JG, Potter S, Moritz C. 2017. Accounting for uncertainty in gene tree estimation: summary-coalescent species tree inference in a challenging radiation of Australian lizards. *Syst Biol*. 66:352–366.

Bryant D, Bouckaert R, Felsenstein J, Rosenberg NA, RoyChoudhury A. 2012. Inferring species trees directly from biallelic genetic markers: bypassing gene trees in a full coalescent analysis. *Mol Biol Evol*. 29:1917–1932.

Chen MY, Liang D, Zhang P. 2017. Phylogenomic resolution of the phylogeny of laurasiatherian mammals: exploring phylogenetic signals within coding and noncoding sequences. *Genome Biol Evol*. 9:1998–2012.

Chen L, Qiu Q, Jiang Y, Wang K, Lin Z, Li Z, Bibi F, Yang Y, Wang J, Nie W, et al. 2019. Large-scale ruminant genome sequencing provides insights into their evolution and distinct traits. *Science*. 364:eaav6202.

Chifman J, Kubatko L. 2014. Quartet inference from SNP data under the coalescent model. *Bioinformatics*. 30:3317–3324.

Chifman J, Kubatko L. 2015. Identifiability of the unrooted species tree topology under the coalescent model with time-reversible substitution processes, site-specific rate variation, and invariable sites. *J Theoret Biol*. 374:35–47.

Chou J, Gupta A, Yaduvanshi S, Davidson R, Nute M, Mirarab S, Warnow T. 2015. A comparative study of SVDquartets and other coalescent-based species tree estimation methods. *BMC Genomics*. 16 (Suppl 10):S2.

Chuong EB, Elde NC, Feschotte C. 2017. Regulatory activities of transposable elements: from conflicts to benefits. *Nat Rev Genet*. 18:71–86.

Churakov G, Kriegs JO, Baertsch R, Zemann A, Brosius J, Schmitz J. 2009. Mosaic retroposon insertion patterns in placental mammals. *Genome Res*. 19:868–875.

Cloutier A, Sackton TB, Grayson P, Clamp M, Baker AJ, Edwards SV. 2019. Whole-genome analyses resolve the phylogeny of flightless birds (Palaeognathae) in the presence of an empirical anomaly zone. *Syst Biol*. 68:937–955.

Degnan JH. 2013. Anomalous unrooted gene trees. *Syst Biol*. 62:574–590.

Degnan JH, Rosenberg NA. 2006. Discordance of species trees with their most likely gene trees. *PLoS Genet*. 2:e68.

Degnan JH, Rosenberg NA. 2009. Gene tree discordance, phylogenetic inference and the multispecies coalescent. *Trends Ecol Evol*. 24:332–340.

Deininger PL, Batzer MA. 2002. Mammalian retroelements. *Genome Res*. 12:1455–1465.

Dekel Y, Machluf Y, Ben-Dor S, Yifa O, Stoler A, Ben-Shlomo I, Bercovich D. 2015. Dispersal of an ancient retroposon in the TP53 promoter of Bovidae: phylogeny, novel mechanisms, and potential implications for cow milk persistency. *BMC Genomics*. 16:53.

Deméré TA, McGowen MR, Berta A, Gatesy J. 2008. Morphological and molecular evidence for a stepwise evolutionary transition from teeth to baleen in mysticete whales. *Syst Biol*. 57:15–37.

D'Erchia AM, Gissi C, Pesole G, Saccone C, Arnason U. 1996. The guinea pig is not a rodent. *Nature*. 381:597–600.

Doronina L, Churakov G, Kuritzin A, Shi J, Baertsch R, Clawson H, Schmitz J. 2017a. Speciation network in Laurasiatheria: retrophylogenomic signals. *Genome Res*. 27:997–1003.

Doronina L, Churakov G, Shi J, Brosius J, Baertsch R, Clawson H, Schmitz J. 2015. Exploring massive incomplete lineage sorting in arctoids (Laurasiatheria, Carnivora). *Mol Biol Evol*. 32:3194–3204.

Doronina L, Matzke A, Churakov G, Stoll M, Huge A, Schmitz A. 2017b. The beaver's phylogenetic lineage illuminated by retroposon reads. *Sci Rep*. 7:43562.

Doronina L, Reising O, Clawson H, Ray DA, Schmitz J. 2019. True homoplasy of retrotransposon insertions in primates. *Syst Biol*. 68:482–493.

dos Reis M, Inoue J, Hasegawa M, Asher RJ, Donoghue PC, Yang Z. 2012. Phylogenomic datasets provide both precision and accuracy in estimating the timescale of placental mammal phylogeny. *Proc Biol Sci*. 279:3491–3500.

Doyle JJ. 1992. Gene trees and species trees: molecular systematics as one-character taxonomy. *Syst Bot*. 17:144–163.

Doyle JJ. 1997. Trees within trees: genes and species, molecules and morphology. *Syst Biol*. 46:537–553.

Durand EY, Patterson N, Reich D, Slatkin M. 2011. Testing for ancient admixture between closely related populations. *Mol Biol Evol*. 28:2239–2252.

Emerling CA, Huynh HT, Nguyen MA, Meredith RW, Springer MS. 2015. Spectral shifts of mammalian ultraviolet-sensitive pigments (short wavelength-sensitive opsin 1) are associated with eye length and photic niche evolution. *Proc Roy Soc B*. 282:20151817.

Feijoo M, Parada A. 2017. Macrosystematics of eutherian mammals combining HTS data to expand taxon coverage. *Mol Phylogenet Evol*. 113:76–83.

Felsenstein J. 1979. Alternative methods of phylogenetic inference and their interrelationship. *Syst Biol*. 28:49–62.

Foley NM, Springer MS, Teeling EC. 2016. Mammal madness: is the mammal tree of life not yet resolved. *Philos Trans R Soc Lond B Biol Sci*. 371:20150140.

Gaetano J. 2018. Holm–Bonferroni sequential correction: an EXCEL calculator (1.3) [Microsoft Excel workbook]. Available from: https://bit.ly/2VQOqcn

Gatesy J, Geisler JH, Chang J, Buell C, Berta A, Meredith RW, Springer MS, McGowen MR. 2013. A phylogenetic blueprint for a modern whale. *Mol Phylogenet Evol*. 66:479–506.

Gatesy J, Meredith RW, Janecka JE, Simmons MP, Murphy WJ, Springer MS. 2017. Resolution of a concatenation/coalescence kerfuffle: partitioned coalescence support and a robust family-level tree for Mammalia. *Cladistics*. 33:295–332.

Gatesy J, Sloan DB, Warren JM, Baker RH, Simmons MP, Springer MS. 2019. Partitioned coalescence support reveals biases in species-tree methods and detects gene trees that determine phylogenomic conflicts. *Mol Phylogenet Evol*. 139:106539.

Gatesy J, Springer MS. 2013. Concatenation versus coalescence versus "concatalescence". *Proc Natl Acad Sci U S A*. 110:E1179.

Gatesy J, Springer MS. 2014. Phylogenetic analysis at deep timescales: unreliable gene trees, bypassed hidden support, and the coalescence/concatalescence conundrum. *Mol Phylogenet Evol*. 80:231–266.

Gatesy J, Springer MS. 2017. Phylogenomic red flags: homology errors and zombie lineages in the evolutionary diversification of placental mammals. *Proc Natl Acad Sci U S A*. 114:E9431–9432.

Graur D, Hide WA, Li WH. 1991. Is the guinea-pig a rodent? *Nature*. 351:649–652.

Graybeal A. 1998. Is it better to add taxa or characters to a difficult phylogenetic problem? *Syst Biol*. 47:9–17.

Green RE, Krause J, Briggs AW, Maricic T, Stenzel U, Kircher M, Patterson N, Li H, Zhai W, Fritz MH, *et al*. 2010. A draft sequence of the Neandertal genome. *Science*. 328:710–722.

Guindon S, Dufayard JF, Lefort V, Anisimova M, Hordijk W, Gascuel O. 2010. New algorithms and methods to estimate maximum-likelihood phylogenies: assessing the performance of PhyML 3.0. *Syst Biol*. 59:307–321.

Hallström BM, Schneider A, Zoller S, Janke A. 2011. A genomic approach to examine the complex evolution of laurasiatherian mammals. *PLoS One*. 6:e28199.

Han KL, Braun EL, Kimball RT, Reddy S, Bowie RC, Braun MJ, Chojnowski JL, Hackett SJ, Harshman J, Huddleston CJ, *et al.* 2011. Are transposable element insertions homoplasy free? An examination using the avian tree of life. *Syst Biol*. 60:375–386.

Hartig G, Churakov G, Warren WC, Brosius J, Makałowski W, Schmitz J. 2013. Retrophylogenomics place tarsiers on the evolutionary branch of anthropoids. *Sci Rep*. 3:1756.

Hillis DM. 1996. Inferring complex phylogenies. *Nature*. 383:130–131.

Holm S. 1979. A simple sequentially rejective multiple test procedure. *Scand J Stat*. 6:65–70.

Houde P, Braun EL, Narula N, Minjares U, Mirarab S. 2019. Phylogenetic signal of indels and the neoavian radiation. *Diversity*. 11:108.

Huang H, He Q, Kubatko LS, Knowles LL. 2010. Sources of error inherent in species-tree estimation: impact of mutational and coalescent effects on accuracy and implications for choosing among different methods. *Syst Biol*. 59:573–583.

Huang H, Knowles LL. 2009. What is the danger of the anomaly zone for empirical phylogenetics? *Syst Biol*. 58:527–536.

Hudson RR. 1990. Gene genealogies and the coalescent process. *Oxford Surv Evol Biol.* 7:1–44.

Huson DH, Bryant D. 2006. Application of phylogenetic networks in evolutionary studies. *Mol Biol Evol*. 23:254–267.

Huson DH, Klöpper TH, Lockhart PJ, Steel MA. 2005. Reconstruction of reticulate networks from gene trees. In: Miyano S, Mesirov J, Kasif S, Istrail S, Pevzner P, Waterman M, editors. *Research in computational biology. Lecture notes in computer science*. Vol. 3500. Berlin: Springer-Verlag. p. 233–249.

Jarvis ED, Mirarab S, Aberer AJ, Li B, Houde P, Li C, Ho SY, Faircloth BC, Nabholz B, Howard JT, *et al.* 2014. Whole-genome analyses resolve early branches in the tree of life of modern birds. *Science*. 346:1320–1331.

Jiang T, Kearney P, Li M. 2000. A polynomial time approximation scheme for inferring evolutionary trees from quartet topologies and its application. *SIAM J Comput*. 30:1942–1961.

Johnson WE. 2019. Origins and evolutionary consequences of ancient endogenous retroviruses. *Nat Rev Microbiol*. 17:355–370.

Kubiak MR, Makalowska I. 2017. Protein-coding genes' retrocopies and their functions. *Viruses* 9:80.

Kuritzin A, Kischka T, Schmitz J, Churakov G. 2016. Incomplete lineage sorting and hybridization statistics for large-scale retroposon insertion data. *PLoS Comput Biol.* 12:e1004812.

Lammers F, Blumer M, Rücklé C, Nilsson MA. 2019. Retrophylogenomics in rorquals indicate large ancestral population sizes and a rapid radiation. *Mob DNA*. 10:5.

Lander ES, Linton LM, Birren B, Nusbaum C, Zody MC, Baldwin J, Devon K, Dewar K, Doyle M, FitzHugh W, *et al.*; International Human Genome Sequencing Consortium. 2001. Initial sequencing and analysis of the human genome. *Nature*. 409:860–921.

Li G, Davis BW, Eizirik E, Murphy WJ. 2016. Phylogenomic evidence for ancient hybridization in the genomes of living cats (Felidae). *Genome Res*. 26:1–11.

Li G, Figueiró HV, Eizirik E, Murphy WJ. 2019. Recombination-aware phylogenomics reveals the structured genomic landscape of hybridizing cat species. *Mol Biol Evol*. 36:2111–2126.

Liang B, Wang N, Li N, Kimball RT, Braun EL. 2018. Comparative genomics reveals a burst of homoplasy-free numt insertions. *Mol Biol Evol*. 35:2060–2064.

Liu L, Yu L, Edwards SV. 2010. A maximum pseudo-likelihood approach for estimating species trees under the coalescent model. *BMC Evol Biol*. 10:302.

Liu L, Yu L, Kubatko L, Pearl DK, Edwards SV. 2009. Coalescent methods for estimating phylogenetic trees. *Mol Phylogenet Evol.* 53:320–328.

Liu L, Zhang J, Rheindt FE, Lei F, Qu Y, Wang Y, Zhang Y, Sullivan C, Nie W, Wang J, *et al.* 2017. Genomic evidence reveals a radiation of placental mammals uninterrupted by the KPg boundary. *Proc Natl Acad Sci U S A*. 114:E7282–E7290.

Longo SJ, Faircloth BC, Meyer A, Westneat MW, Alfaro ME, Wainwright PC. 2017. Phylogenomic analysis of a rapid radiation of misfit fishes (Syngnathiformes) using ultraconserved elements. *Mol Phylogenet Evol.* 113:33–48.

Maddison WP. 1997. Gene trees in species trees. *Syst Biol*. 46:523–536.

Marx F. 2010. The more the merrier? A large cladistic analysis of mysticetes, and comments on the transition from teeth to baleen. *J Mammal Evol*. 18:77–100.

Marx FG, Fordyce RE. 2015. Baleen boom and bust: a synthesis of mysticete phylogeny, diversity and disparity. *R Soc Open Sci*. 2:140434.

McCormack JE, Faircloth BC, Crawford NG, Gowaty PA, Brumfield RT, Glenn TC. 2012. Ultraconserved elements are novel phylogenomic markers that resolve placental mammal phylogeny when combined with species-tree analysis. *Genome Res*. 22:746–754.

McGowen MR, Spaulding M, Gatesy J. 2009. Divergence date estimation and a comprehensive molecular tree of extant cetaceans. *Mol Phylogenet Evol*. 53:891–906.

Mendes FK, Livera AP, Hahn MW. 2019. The perils of intralocus recombination for inferences of molecular convergence. *Philos Trans R Soc Lond B Biol Sci*. 374:20180244.

Meredith RW, Janečka JE, Gatesy J, Ryder OA, Fisher CA, Teeling EC, Goodbla A, Eizirik E, Simão TL, Stadler T, *et al.* 2011. Impacts of the Cretaceous Terrestrial Revolution and KPg extinction on mammal diversification. *Science*. 334:521–524.

Mirarab S, Bayzid MS, Warnow T. 2014a. Evaluating summary methods for multilocus species tree estimation in the presence of incomplete lineage sorting. *Syst Biol*. 65:366–380.

Mirarab S, Reaz R, Bayzid MS, Zimmermann T, Swenson MS, Warnow T. 2014b. ASTRAL: genome-scale coalescent-based species tree estimation. *Bioinformatics*. 30:i541–i548.

Mirarab S, Warnow T. 2015. ASTRAL-II: coalescent-based species tree estimation with many hundreds of taxa and thousands of genes. *Bioinformatics*. 31:i44–i52.

Molloy EK, Warnow T. 2018. To include or not to include: the impact of gene filtering on species tree estimation methods. *Syst Biol*. 67:285–303.

Morgan CC, Foster PG, Webb AE, Pisani D, McInerney JO, O'Connell MJ. 2013. Heterogeneous models place the root of the placental mammal phylogeny. *Mol Biol Evol.* 30:2145–2156.

Murphy WJ, Eizirik E, O'Brien SJ, Madsen O, Scally M, Douady CJ, Teeling E, Ryder OA, Stanhope MJ, de Jong WW, *et al.* 2001. Resolution of the early placental mammal radiation using Bayesian phylogenetics. *Science*. 294:2348–2351.

Nikaido M, Hamilton H, Makino H, Sasaki T, Takahashi K, Goto M, Kanda N, Pastene LA, Okada N; SMBE Tri-National Young Investigators. 2006. Proceedings of the SMBE Tri-National Young Investigators' Workshop 2005. Baleen whale phylogeny and a past extensive radiation event revealed by SINE insertion analysis. *Mol Biol Evol*. 23:866–873.

Nikaido M, Matsuno F, Hamilton H, Brownell RL Jr, Cao Y, Ding W, Zuoyan Z, Shedlock AM, Fordyce RE, Hasegawa M, *et al.* 2001. Retroposon analysis of major cetacean lineages: the monophyly of toothed whales and the paraphyly of river dolphins. *Proc Natl Acad Sci U S A*. 98:7384–7389.

Nikaido M, Rooney AP, Okada N. 1999. Phylogenetic relationships among cetartiodactyls based on insertions of short and long interpersed elements: hippopotamuses are the closest extant relatives of whales. *Proc Natl Acad Sci U S A*. 96:10261–10266.

Nilsson MA, Churakov G, Sommer M, Tran NV, Zemann A, Brosius J, Schmitz J. 2010. Tracking marsupial evolution using archaic genomic retroposon insertions. *PLoS Biol.* 8:e1000436.

Nilsson MA, Klassert D, Bertelsen MF, Hallström BM, Janke A. 2012. Activity of ancient RTE retroposons during the evolution of cows, spiral-horned antelopes, and Nilgais (Bovinae). *Mol Biol Evol*. 29:2885–2888.

Nishihara H, Hasegawa M, Okada N. 2006. Pegasoferae, an unexpected mammalian clade revealed by tracking ancient retroposon insertions. *Proc Natl Acad Sci U S A*. 103:9929–9934.

Nishihara H, Maruyama S, Okada N. 2009. Retroposon analysis and recent geological data suggest near-simultaneous divergence of the three superorders of mammals. *Proc Natl Acad Sci U S A*. 106:5235–5240.

Patel S, Kimball RT, Braun EL. 2013. Error in phylogenetic estimation for bushes in the tree of life. *J. Phylogenet Evol Biol.* 1:110.

Pease JB, Brown JW, Walker JF, Hinchliff CE, Smith SA. 2018. Quartet sampling distinguishes lack of support from conflicting support in the green plant tree of life. *Am J Bot*. 105:385–403.

Pease JB, Hahn MW. 2015. Detection and polarization of introgression in a five-taxon phylogeny. *Syst Biol*. 64:651–662.

Prum RO, Berv JS, Dornburg A, Field DJ, Townsend JP, Lemmon EM, Lemmon AR. 2015. A comprehensive phylogeny of birds (Aves) using targeted next-generation DNA sequencing. *Nature*. 526:569–573.

Ragan MA. 1992. Phylogenetic inference based on matrix representation of trees. *Mol Phylogenet Evol*. 1:53–58.

Ray DA, Xing J, Salem AH, Batzer MA. 2006. SINEs of a nearly perfect character. *Syst Biol*. 55:928–935.

Reaz R, Bayzid MS, Rahman MS. 2014. Accurate phylogenetic tree reconstruction from quartets: a heuristic approach. *PLoS One*. 9:e104008.

Robinson TJ, Ruiz-Herrera A, Avise JC. 2008. Hemiplasy and homoplasy in the karyotypic phylogenies of mammals. *Proc Natl Acad Sci U S A*. 105:14477–14481.

Roch S, Warnow T. 2015. On the robustness to gene tree estimation error (or lack thereof) of coalescent-based species tree methods. *Syst Biol*. 64:663–676.

Rogers J, Raveendran M, Harris RA, Mailund T, Leppälä K, Athanasiadis G, Schierup MH, Cheng J, Munch K, Walker JA, *et al.*; Baboon Genome Analysis Consortium. 2019. The comparative genomics and complex population history of *Papio* baboons. *Sci Adv*. 5:eaau6947.

Rokas A, Holland PW. 2000. Rare genomic changes as a tool for phylogenetics. *Trends Ecol Evol*. 15:454–459.

Romiguier J, Ranwez V, Delsuc F, Galtier N, Douzery EJ. 2013. Less is more in mammalian phylogenomics: AT-rich genes minimize tree conflicts and unravel the root of placental mammals. *Mol Biol Evol*. 30:2134–2144.

Rosenberg NA. 2013. Discordance of species trees with their most likely gene trees: a unifying principle. *Biol Evol*. 30:2709–2713.

Rosenberg NA, Tao R. 2008. Discordance of species trees and their most likely gene trees: the case of five taxa. *Syst Biol*. 57:131–140.

Rychel AL, Reeder TW, Berta A. 2004. Phylogeny of mysticete whales based on mitochondrial and nuclear data. *Mol Phylogenet Evol*. 32:892–901.

Sackton TB, Grayson P, Cloutier A, Hu Z, Liu JS, Wheeler NE, Gardner PP, Clarke JA, Baker AJ, Clamp M, *et al.* 2019. Convergent regulatory evolution and loss of flight in paleognathous birds. *Science*. 364:74–78.

Sasaki T, Nikaido M, Hamilton H, Goto M, Kato H, Kanda N, Pastene L, Cao Y, Fordyce R, Hasegawa M, *et al.* 2005. Mitochondrial phylogenetics and evolution of mysticete whales. *Syst Biol*. 54:77–90.

Sayyari E, Mirarab S. 2016. Fast coalescent-based computation of local branch support from quartet frequencies. *Mol Biol Evol*. 33:1654–1668.

Sayyari E, Whitfield JB, Mirarab S. 2017. Fragmentary gene sequences negatively impact gene tree and species tree reconstruction. *Mol Biol Evol*. 34:3279–3291.

Schull JK, Turakhia Y, Dally WJ, Bejerano G. 2019. Champagne: whole-genome phylogenomic character matrix method places Myomorpha basal in Rodentia. *bioRxiv*. 803957.

Scornavacca C, Galtier N. 2017. Incomplete lineage sorting in mammalian phylogenomics. *Syst Biol*. 66:112–120.

Shedlock AM, Milinkovitch MC, Okada N. 2000. SINE evolution, missing data, and the origin of whales. *Syst Biol*. 49:808–817.

Shedlock AM, Okada N. 2000. SINE insertions: powerful tools for molecular systematics. *Bioessays*. 22:148–160.

Shedlock AM, Takahashi K, Okada N. 2004. SINEs of speciation: tracking lineages with retroposons. *Trends Ecol Evol*. 19:545–553.

Shimamura M, Yasue H, Ohshima K, Abe H, Kato H, Kishiro T, Goto M, Munechika I, Okada N. 1997. Molecular evidence from retroposons that whales form a clade within even-toed ungulates. *Nature*. 388:666–670.

Simmons MP, Gatesy J. 2015. Coalescence vs. concatenation: sophisticated analyses vs. first principles applied to rooting the angiosperms. *Mol Phylogenet Evol*. 91:98–122.

Simmons MP, Kessenich J. 2019. Divergence and support among slightly suboptimal likelihood gene trees. *Cladistics*. doi:10.1111/cla.12404

Simmons MP, Norton AP. 2014. Divergent maximum-likelihood-branch-support values for polytomies. *Mol Phylogenet Evol*. 73:87–96.

Simmons MP, Randle CP. 2014. Disparate parametric branch-support values from ambiguous characters. *Mol Phylogenet Evol*. 78:66–86.

Simmons MP, Sloan DB, Springer MS, Gatesy J. 2019. Gene-wise resampling outperforms site-wise resampling in phylogenetic coalescence analyses. *Mol Phylogenet Evol*. 131:80–92.

Slatkin M, Pollack JL. 2008. Subdivision in an ancestral species creates asymmetry in gene trees. *Mol Biol Evol*. 25:2241–2246.

Snir S, Rao S. 2012. Quartet MaxCut: a fast algorithm for amalgamating quartet trees. *Mol Phylogenet Evol*. 62:1–8.

Solís-Lemus C, Yang M,Ané C. 2016. Inconsistency of species tree methods under gene flow. *Syst Biol*. 65:843–851.

Song S, Liu L, Edwards SV, Wu S. 2012. Resolving conflict in eutherian mammal phylogeny using phylogenomics and the multispecies coalescent model. *Proc Natl Acad Sci U S A*. 109:14942–14947.

Springer MS, Foley NM, Brady PL, Gatesy J, Murphy WJ. 2019. Evolutionary models for the diversification of placental mammals across the KPg boundary. *Front Genet*. 10:1241.

Springer MS, Gatesy J. 2014. Land plant origins and coalescence confusion. *Trends Plant Sci*. 19:267–269.

Springer MS, Gatesy J. 2016. The gene tree delusion. *Mol Phylogenet Evol*. 94:1–33.

Springer MS, Gatesy J. 2017. Pinniped diphyly and bat triphyly: more homology errors drive conflicts in the mammalian tree. *J Hered*. 109: 297–307.

Springer MS, Gatesy J. 2018a. Delimiting coalescence genes (c-genes) in phylogenomic data sets. *Genes*. 9:123.

Springer MS, Gatesy J. 2018b. On the illogic of coalescence simulations for distinguishing the causes of conflict among gene trees. *J Phylogenet Evol Biol*. 6:3.

Springer MS, Gatesy J. 2018c. On the importance of homology in the age of phylogenomics. *Syst Biodivers*. 16:210–228.

Steeman ME, Hebsgaard MB, Fordyce RE, Ho SY, Rabosky DL, Nielsen R, Rahbek C, Glenner H, Sørensen MV, Willerslev E. 2009. Radiation of extant cetaceans driven by restructuring of the oceans. *Syst Biol*. 58:573–585.

Suh A, Paus M, Kiefmann M, Churakov G, Franke FA, Brosius J, Kriegs JO, Schmitz J. 2011. Mesozoic retroposons reveal parrots as the closest living relatives of passerine birds. *Nat Commun*. 2:443.

Suh A, Smeds L, Ellegren H. 2015. The dynamics of incomplete lineage sorting across the ancient adaptive radiation of neoavian birds. *PLoS Biol*. 13:e1002224.

Sukumaran J, Holder MT. 2010. DendroPy: a Python library for phylogenetic computing. *Bioinformatics*. 26:1569–1571.

Swofford DL. 2002. PAUP*. Phylogenetic analysis using parsimony (* and other methods). Sunderland (MA): Sinauer Associates.

Tarver JE, Dos Reis M, Mirarab S, Moran RJ, Parker S, O'Reilly JE, King BL, O'Connell MJ, Asher RJ, Warnow T, *et al.* 2016. The interrelationships of placental mammals and the limits of phylogenetic inference. *Genome Biol Evol*. 8:330–344.

Vachaspati P, Warnow T. 2018a. SVDquest: improving SVDquartets species tree estimation using exact optimization within a constrained search space. *Mol Phylogenet Evol*. 124:122–136.

Vachaspati P, Warnow T. 2018b. SIESTA: enhancing searches for optimal supertrees and species trees. *BMC Genomics*. 19:252.

Waddell PJ, Kishino H, Ota R. 2001. A phylogenetic foundation for comparative mammalian genomics. *Genome Inform*. 12:141–154.

Wenzel JW, Siddall ME. 1999. Noise. *Cladistics*. 15:51–64.

Yonezawa T, Segawa T, Mori H, Campos PF, Hongoh Y, Endo H, Akiyoshi A, Kohno N, Nishida S, Wu J, *et al.* 2017. Phylogenomics and morphology of extinct paleognaths reveal the origin and evolution of the ratites. *Curr Biol*. 27:68–77.

Yu Y, Dong J, Liu KJ, Nakhleh L. 2014. Maximum likelihood inference of reticulate evolutionary histories. *Proc Natl Acad Sci U S A*. 111:16448–16453.

Yu Y, Than C, Degnan JH, Nakhleh L. 2011. Coalescent histories on phylogenetic networks and detection of hybridization despite incomplete lineage sorting. *Syst Biol*. 60:138–149.

Zhang C, Rabiee M, Sayyari E, Mirarab S. 2018. ASTRAL-III: polynomial time species tree reconstruction from partially resolved gene trees. *BMC Bioinformatics*. 19:153.

Zhang C, Sayyari E, Mirarab S. 2017. ASTRAL-III: increased scalability and impacts of contracting low support branches. In: Meidanis J, Nakhleh L., editors. *Proceedings Comparative Genomics: 15th International Workshop, RECOMB CG 2017*. October 4–6, 2017, Barcelona, Spain. Cham: Springer International Publishing. p. 53–75.

Zhong B, Liu L, Yan Z, Penny D. 2013. Origin of land plants using the multispecies coalescent model. *Trends Plant Sci*. 18:492–495.